國立臺灣大學電機資訊學院光電工程學研究所

碩士論文

Graduate Institute of Photonics and Optoelectronics

College of Electrical Engineering and Computer Science

National Taiwan University

Master Thesis

應用微機電反射鏡之廣角光達系統設計與實現

Design and realization of a wide field-of-view LiDAR system with a micro mirror

林家興

Chia-Hsing Lin

指導教授：蘇國棟 博士

Advisor: Guo-Dung J. Su, Ph.D.

中華民國 109 年 12 月

December, 2020

國立臺灣大學碩士學位論文
口試委員會審定書

應用微機電反射鏡之廣角光達系統設計與實現
Design and realization of a wide field-of-view
LiDAR system with a micro mirror

本論文係林家興君（學號 R07941042）在國立臺灣大學
光電工程學研究所完成之碩士學位論文，於民國 109 年 12
月 18 日承下列考試委員審查通過及口試及格，特此證明

口試委員：

_____ （指導教授）

_____　_____

所　　長　

2

誌謝

感謝培養我長大含辛茹苦的父母，謝謝你們的支持我才能完成本篇論文。

本論文是在蘇國棟老師的親切關懷和悉心指導下完成的，他嚴肅的科學態度，嚴謹的治學精神，精益求精的工作作風，深深地感染和激勵著我。蘇老師不僅在學業上給我以精心指導，同時還在思想、生活上給我以無微不至的關懷，蘇老師多次詢問研究進程，並為我指點迷津，幫助我開拓研究思路，精心點撥、熱忱鼓勵。蘇老師一絲不苟的作風，嚴謹求實的態度，踏踏實實的精神，不僅授我以文，而且教我做人，雖歷時兩年，卻給以終生受益無窮之道。對陸老師的感激之情是無法用言語表達的。在此謹向蘇老師致以誠摯的謝意和崇高的敬意。

另外，我要特別感謝孟珊在我做研究的過程給予很多鼓勵，也對於許多光學方面的知識提供許多建議；感謝建霖學長給我許多做研究的方法，讓我的論文邏輯更臻健全；感謝瑋倫學長在研究上總是盡力的給予協助；感謝宗融在做研究方面給予很多建議；感謝玟澤在研究上提供許多協助。在此表示深深的感謝，沒有他們的幫助和支持是沒有辦法完成我的碩士學位論文的，同窗之間的友誼永遠長存。

最後，再次對關心、幫助我的老師和同學表示衷心地感謝！

i

中文摘要

Light Detection and Ranging (LiDAR)傳感器技術是自動化運輸的主要推動力。透過融合 LiDAR 的傳感器數據、雷達以及相機鏡頭就可以全面而穩健的感知周圍環境。但是，現今的 LiDAR 解決方案大多非常複雜且成本高昂，且無法有效的實現大視場的掃描，因此無法廣泛的應用到車輛與機器人中。

我們模擬並演示了完整的 LiDAR 系統，並透過將微機電反射鏡(MEMS mirror)加入掃瞄系統中，實現低成本、小體積、大視場掃描的 LiDAR 系統。首先，應用 ZEMAX OpticStudio 光學模擬軟體設計整個 LiDAR 掃描系統，包含準直透鏡、MEMS mirror、反射訊號接收透鏡，並在掃描擴角光學上設計一組非球面的光學系統，達到擴大光達掃描角度的目的。雷射光束經過此組廣角透鏡後掃描角度可以擴大 4 倍，達到 100 度。廣角透鏡的 distortion 控制在 3%以下，讓掃描畫面更接近真實情況。第二，為了演示低成本、小體積 MEMS 掃描光達，使用了模組化雷射測距儀(LRF)並加入 MEMS mirror。整個系統架設在自行設計與製作的支撐具上。完整的 LiDAR 掃描儀原型體積小於 150mm*50mm*30mm。重量小於 250 公克。在 2 klux 的自然光環境中對於 wide-angle LiDAR 進行測量分析，最大的誤差為 4.1cm，因此誤差為 2%以內。最後使用自行撰寫的影像處理程式，將掃描數據轉換為 3D 點雲圖，生成的圖像證明了 LiDAR 的完整功能。

關鍵字： 光達、飛行時間、光學系統設計、雷射、廣角掃描、廣角透鏡、可攜式、微機電鏡、點雲圖

ABSTRACT

Light Detection and Ranging (LiDAR) sensor technology will become the main driving force for automated transportation. Through the fusion of LiDAR sensor data, radar and camera lens, the surrounding environment can be fully and robustly sensed. However, most of today's LiDAR solutions are very complex and costly, and cannot effectively achieve large field of view scanning, so they cannot be widely used in vehicles and robots.

We simulated and demonstrated a complete LiDAR system, and by adding Microelectromechanical Systems(MEMS) mirror to the scanning system, we created a low-cost, small size, and large field of view scanning LiDAR system. First, use ZEMAX OpticStudio optical simulation software to design the entire LiDAR scanning system, including collimating lens, MEMS mirror, and reflection signal receiving lens. And design a group of aspherical optical systems on the scanning angle expansion optics to achieve the purpose of expanding the scanning angle of light. After the laser beam passes through this group of wide-angle lenses, the scanning angle can be expanded 4 times to 100 degrees. The distortion of the wide-angle lens is controlled below 3%, making the scanned image closer to the real situation. Second, in order to demonstrate low-cost, small-volume MEMS scanning LiDAR, an OEM module laser rangefinder (LRF) was used and MEMS mirror was added. The entire system is erected on a self-designed and manufactured support. The complete prototype of LiDAR scanner is less than 150mm*50mm*30mm. The weight is less than 250 grams. In the 2 klux natural light environment for wide-angle LiDAR measurement and analysis, the maximum error is 4.1cm, so the error is within 2%. Finally, a self-written image processing program was

used to convert the scanned data into a 3D point cloud image, and the generated image proved the complete function of LiDAR.

CONTENTS

LIST OF FIGURES

LIST OF TABLES

Chapter 1   Introduction

LiDAR is a method of dynamically measuring distance. By measuring the distance of each object in the surrounding environment, LiDAR has many very practical applications. LiDAR was invented in the early 1960s and was first used in meteorology[1]. Then, it has many applications in archaeological investigation and agriculture. In archaeological investigations, LiDAR can help archaeologists collect data on historical sites quickly and at low cost[2]. In agriculture, installing LiDAR on agricultural robots and agricultural aircraft can help classify plant species and analyze their growth status data. In addition, through integration with Geographic Information System (GIS), it can be used for urban environmental planning and archaeological site search. Since the demand for autonomous driving systems (ADAS) has grown this year, LiDAR has frequently appeared in daily life. LiDAR-related applications can be seen everywhere in life. Autonomous vehicles can use the LiDAR system to scan the surrounding environment, identify and detect the driving environment, and perform functions such as collision avoidance and route guidance. By combining with Simultaneous localization and mapping (SLAM) and the Internet of Things (IoT)[3], many manufacturing processes can save a lot of manpower and achieve the goal of reducing costs.

1.1   Time-of-Flight principle

In the LiDAR system, the most important scanning information is the distance between the scanner and the object to be measured. LiDAR uses the laser light to be emitted and then calculates the elapsed time of the light reflected by the object. With the flight time, the distance between the LiDAR and the object to be measured can be inferred.

Since the light can be accurately projected onto the object to be detected after passing through the optical lens, many very practical applications can be designed based on this principle.

In LiDAR systems, phase shift and time-of-flight methods have been applied to distance measurement. In the phase shift method, a light beam with a specific frequency intensity modulated is emitted to the target, and a phase shift is generated according to the distance during reflection[4]. Although the phase shift system can be used for precise measurement, the phase shift requires a complex system, including a laser beam modulation and data processing system. In addition, due to the long measurement time required, it is difficult to actually apply it in daily life. Time-of-flight method is currently the most potential LiDAR measurement method[5], because of its simple structure and low price, it can be applied to many practical applications. The principle of ToF LiDAR will be explained below.

Fig. 1.1 depicts the basic structure and time-of-flight method principle of LiDAR. The central system controller triggers the emission of a laser pulse, which is reflected by the target and finally received by a photodiode. With the help of a fast-running timer, the flight time of the laser pulse calculates the distance between the target and the LiDAR, so as to realize three-dimensional environmental perception.
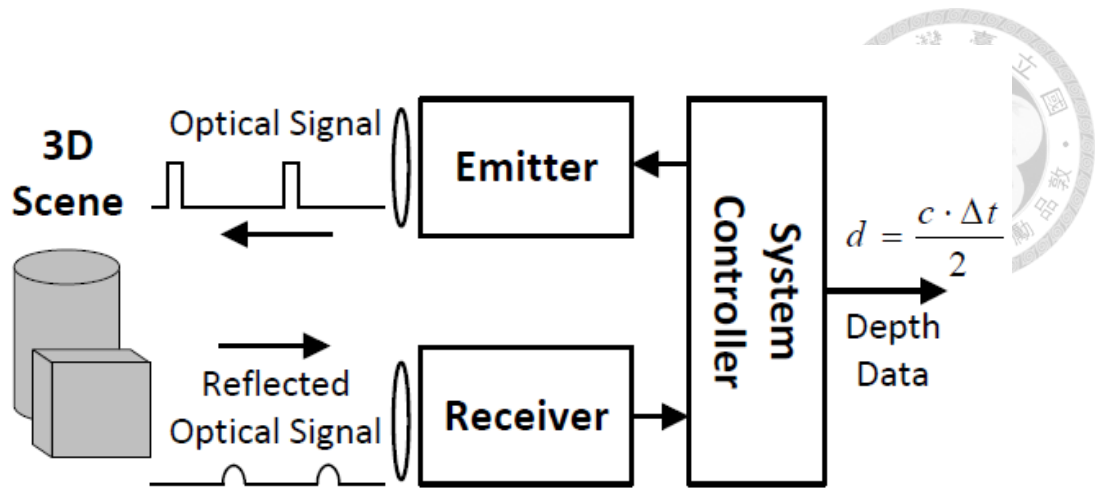
Fig. 1.1　The basic structure and time-of-flight method principle of LiDAR.[6]

As shown in Fig. 1.2, a short-pulse laser is used to generate a short-pulse photon source, and a timer is started while emitting photons. After the photons are scattered back to the photodetector by the object to be measured, the photodetector stops sending signals Timing, this period of time is multiplied by the speed of light and divided by 2 to get the distance of the object to be measured, which is a fairly simple and reliable way of ranging. It can be seen that the pulse light source, light detector, and timer constitute the core part of the single-point optical radar, and then through scanning or array imaging, the function of the 3D optical radar can be completed[7]. In the pulse laser light source, its wavelength must be in the infrared range that is invisible to the human eye to avoid eye damage. The shorter the pulse width, the better, which can provide higher accuracy in distance measurement; in the application of optical distance measurement in vehicles It is usually desirable to increase the sensing distance as much as possible to gain the response time, but because the object under test usually scatters laser light, the number of photons that can return to the detector is greatly reduced. This effect becomes more serious as the distance is farther. Therefore, if you want to increase the measurable distance, you must increase the laser power, but this will cause a heavy burden on the cost of the module and

increase the complexity of the light source drive circuit[8]. Another solution is to use more sensitive light detection. Therefore, single-photon avalanche diode (SPAD) and Avalance Photodiode (APD) are considered as solutions for LiDAR systems to solve the high cost and high complexity of current automotive optical radars[9-11].
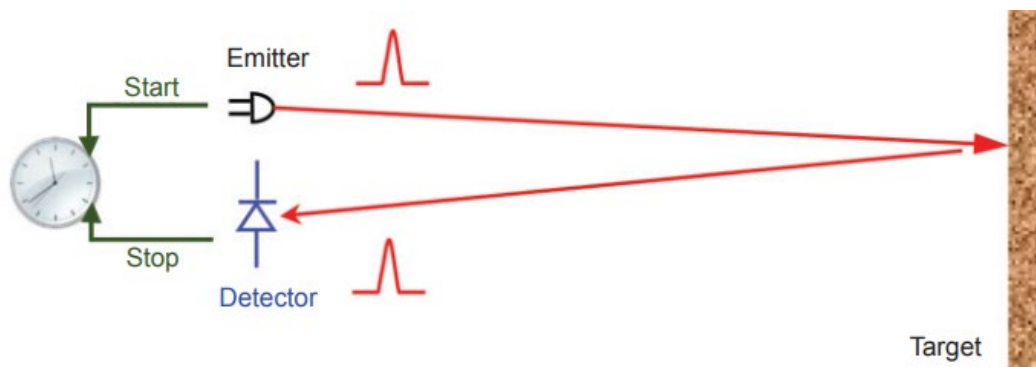
Fig. 1.2 A short-pulse laser is used to generate a short-pulse photon source, and a timer is started while emitting photons.[12]

1.2 Basics of LiDAR imaging

Regarding the technology of detecting the distance of an object, we have always heard of RADAR. This device can calculate the position of objects in space by relying on the bounce of radio waves. Thanks to the growth of electromagnetic wave technology, only in recent years, with the concept of RADAR technology plus some optical principles, researchers have developed a technology that can more accurately measure distance, that is, LiDAR. In other words, the RADAR system emits radio waves and measures the bounce signal. LiDAR uses light waves when measuring distance. Because the data collection capabilities of this system are more powerful, it can provide more practical 3-D information models. LiDAR has a wide range of uses and is suitable for different purposes. Especially in the last five to ten years, many companies and academic circles have begun to focus on this technology[12]. More precisely, LiDAR is a distance

4

measurement method that measures distance through a measuring beam. LiDAR uses pulsed laser light to measure objects and uses extremely accurate detectors to collect the returned signal light. The calculated data can then be used to digitize the surrounding environment to obtain a 3-D representation.
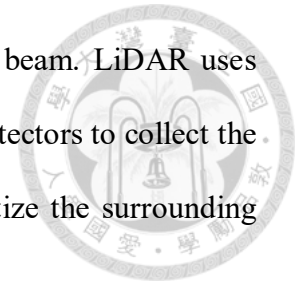
As shown in Fig. 1.3, the beam divergence angle depends on the ratio of the aperture and wavelength of the transmitting antenna (radar) or lens (LiDAR). This ratio is too large for the larger beam divergence angle and smaller angular resolution produced by radar. As shown in the figure above, radar (black dashed line) cannot distinguish between the two vehicles, while LiDAR (red dashed line) can. Radar's angular resolution is low, and he may regard the two closer cars as one large car, thus sending out wrong signals and making identification difficult[13]. The recognition ability of LiDAR is very high, and pedestrian gestures from tens of meters away can be easily recognized.
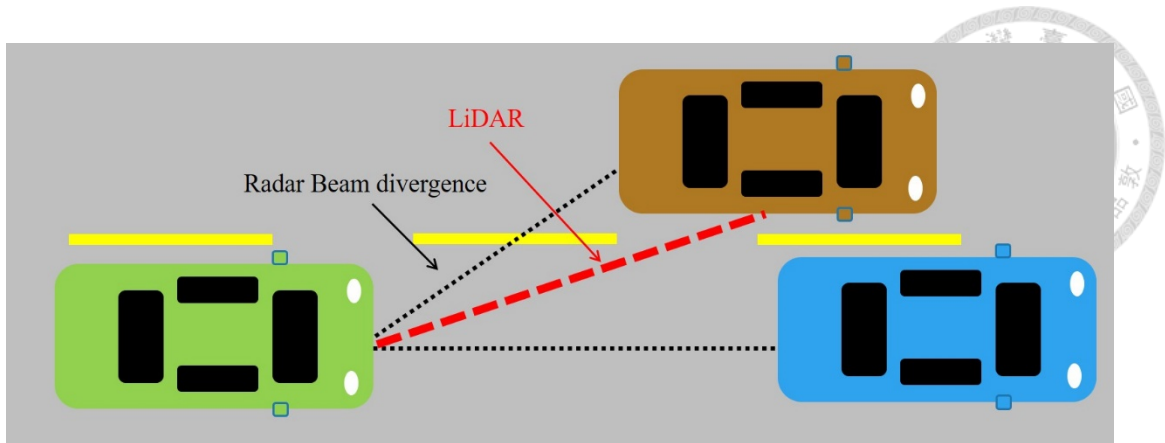
Fig. 1.3   Schematic diagram of LiDAR and RADAR application in autonomous driving. Radar's angular resolution is low, and it may treat two closer cars as one large car, thus sending out wrong signals and making identification difficult. The recognition ability of LiDAR is very high, pedestrian gestures from tens meters away can be easily recognized.
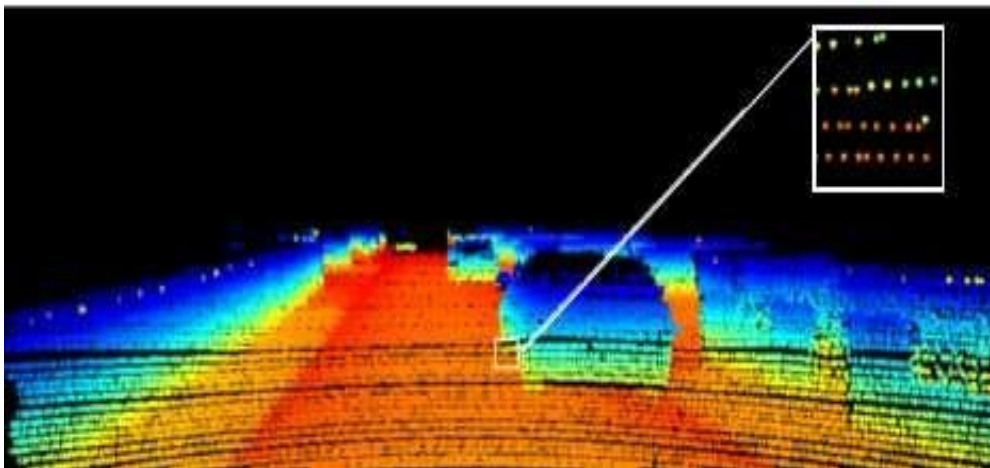
Fig. 1.4   Depth image example. Through the depth image, we can know the distance between each object and the scanner directly from the image.[14]
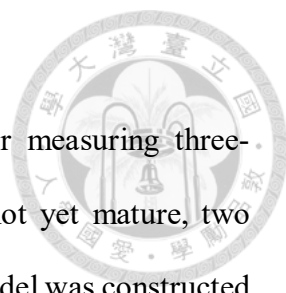
LiDAR mostly uses infrared light to image objects. It can detect many target objects, including cars, rocks, non-metallic materials, rain, clouds, aerosol, and even single chemical molecules[12, 15, 16]. But we must keep one thing in mind, because LiDAR uses the reflected light signal from the surface of the object to image, so we can only

6

understand the surface of the target, but cannot penetrate the object. Therefore, it cannot penetrate dense smoke. In any case, the laser beam can present the uneven surface of the object with a high resolution. The beam reflection signal collected by LiDAR is not pure reflection, but there are many types of scattering, the most common is Rayleigh scattering[17].
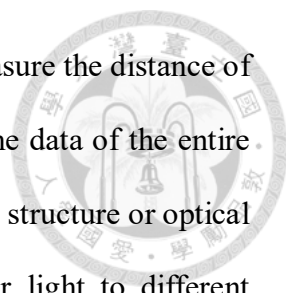
Through LiDAR, we can get the distance between the light source and the target object. At this time, the obtained detection data is in one-dimensional form, that is, many different distance data will be received. Through the processing of the image processing program, the obtained distance data can be converted into a three-dimensional image. The denser the data points can form a more accurate model, or use the SP-line mathematical calculation method to reconstruct the surface shape of the object[10, 12]. This process is called 3D reconstruction. Unlike a camera, the image formed by LiDAR has depth data, also called depth image[18, 19]. The camera only captures the color information in the space. With the technology that can detect the distance of objects, this technology can be used in many places. For example, autonomous driving, robotics, factory automation, etc.
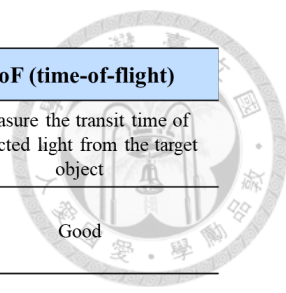
Fig. 1.5　Application of LiDAR in ADAS system.[2]

7

Three-dimensional measurement is a traditional technique for measuring three-dimensional images in space. When the LiDAR technology was not yet mature, two cameras were used to shoot left and right, and a three-dimensional model was constructed using visual stereo imaging. After filmmakers used high-definition cameras to make 3D movies many years ago, many 3D imaging products entered the consumer market. In recent years, due to the improvement of mobile phone performance, many game manufacturers have launched games with 3-D display functions, which greatly increases the demand for 3-D measurement technology. The other three requirements for measurement are industrial manufacturing industries, such as industrial inspection, reverse engineering, robots, and automatic vehicles[20]. In the process of monitoring and automation that requires higher precision, traditional measurement methods can no longer meet today's needs. Imaging measurement size and target recognition require better hardware architecture to achieve higher resolution and computing speed. When moving like a mobile robot, it requires three-dimensional measurement of the environment map, real-time dynamic scanning of the scene, simultaneous localization and mapping (SLAM)[21]. When the automatic driving system or robot moves, it uses the geometric features (edges, angles) of environmental objects to locate its own position, so that it can grasp the relative position of adjacent objects, such as walls, pillars, road trees, etc., and move instantly. If there are only two-dimensional images, it is difficult to correctly perceive the real spatial relationship between the environment and the object, and the system cannot make correct decisions and actions. Therefore, in addition to traditional 3D film and television products or reverse reconstruction engineering applications, 3D measurement has become a key technology in industries such as automation, robotics, and self-driving cars.

In ToF LiDAR measurement, the laser light source can only measure the distance of a single point from emission to reception. If you want to measure the data of the entire spatial range, you need to deflect the beam through some mechanical structure or optical technology. There are many different methods to deflect the laser light to different positions to scan the complete field of view. The method of deflecting laser light will be explained in detail in chapter 2.2. But when reconstructing a 3D image, you need to know the relative position of each data point in space. By combining the data of each signal with the scanning position, that is, combining the distance and the data of the x-axis, y-axis and z-axis in the space, all the data points can be integrated into a point cloud diagram that is convenient for observation.

	Stereoscopic vision	Structured light	ToF (time-of-flight)
Principle	Compare disparities of stereo images from two 2D sensors	Detect distortions of illuminated patterns by 3D surface	Measure the transit time of reflected light from the target object
Low light performance	Weak	Good	Good
Bright light performance	Good	Weak/medium (depends on illumination power)	Medium
Material cost	Low	Middle/high	Middle
Depth accuracy	mm to cm (difficulty with smooth and non-textured surface)	μm to mm (depends on the pattern density)	mm to cm (depends on resolution of ToF sensor)
Image resolution	High (camera dependent)	High (camera dependent)	Medium (ToF sensor size dependent)
Distance range	Mid range (depends on the distance between two cameras)	Very short to mid range (depends on illumination power)	Short to long range (depends on laser power and modulation)
Scanning speed	Medium (limited by software complexity)	Medium/Fast (limited by SW complexity and camera speed)	Fast (limited by sensor speed)

Table 1.1 Comparison of three 3D imaging methods.

1.3   LiDAR applications

LiDAR originated in the early 1960s. That is, not long after the invention of the laser, LiDAR technology began to grow. Combined with laser imaging technology, distance can be measured quickly by using appropriate sensors and data acquisition electronics. The first application of LiDAR was meteorology, and the National Center for Atmospheric Research used it to measure cloud cover to improve the accuracy of weather forecasts. What really made LiDAR famous was in 1971, during NASA's Apollo 15 space mission, a set of laser measurement systems were designed for astronauts to measure the height of the moon's surface. The initial applications of LiDAR are mainly archaeology, geography,

geology, geomorphology, geodesy, biology, atmosphere and other fields. These applications are related to high-density, high-power laser beams. But now LiDAR is developing in the opposite direction. People have developed many low-power laser beam applications in order to pay more attention to the lightness of the equipment and human eye safety[22]. Considering that low-power LiDAR can be used for short-distance scanning, object position detection and 3-D object surface scanning, these technologies are developed in areas such as autonomous driving and robotics[23]. Next we will discuss the application of LiDAR in different fields.

1.3.1   Terrestrial LiDAR

Terrestrial LiDAR is also called Terrestrial laser scanning, which can be divided into fixed and mobile. Fixed ground scanning is the most common ground survey method, which is often used in geography and cultural heritage surveys. From this type of laser scanning instrument, we can get a 3-D point cloud map, which is linked with the actual location location point to create a realistic terrain appearance. Compared with other technologies, Terrestrial LiDAR can perform 3-D model modeling in a short time[24].

The mobile Terrestrial LiDAR uses two or more LiDARs and is installed on a moving vehicle to collect data along the route. These instruments must be paired with positioning systems. Terrestrial LiDAR 3-D point cloud image will be used with grid map generation calculation method. By cutting a series of z-axis point information into many grids, the LiDAR data corresponds to the respective grids. This technology is needed for street surveying, road wiring configuration and bridge construction. From the 3-D point cloud diagram, engineers can quickly understand the actual location of all objects on the ground, such as the height of the bridge, the size of the surrounding trees and other data, as shown in Fig. 1.6. By capturing data directly from the point cloud, construction

efficiency can be greatly improved.
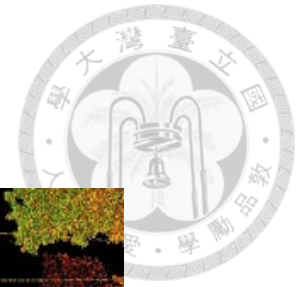
Fig. 1.6　Use Terrestrial LiDAR to scan the building and reconstruct the three-dimensional model of the building.[38]

1.3.2　Airborne LiDAR

Airborne LiDAR creates a 3-D point cloud model from a bird's-eye perspective by combining LiDAR with an aircraft , as shown in Fig. 1.7. This is the most detailed and accurate method for modeling landform undulations and can replace aerial photography. Professional Airborn LiDAR is compared with photogrammetry, Airborne LiDAR can clearly create mathematical models of surface information, such as rivers, roads, houses, etc. Airborne LiDAR can also be used for shallower water measurement, which can quickly obtain depth information. In the past, Airborne LiDAR is usually very large and consumes a lot of power, so a large aircraft is required to carry it[25]. However, in recent years, due to the continuous development of LiDAR scanning technology, Airborne LiDAR has been reduced to the extent that it can be installed on small drones. This greatly reduces the threshold for using Airborne LiDAR. Researchers can perform aerial laser

scanning on their own at a very low price[26].

Fig. 1.7   Use airborne LiDAR to scan the ground.[39]

1.3.3   Urban Planning

In the era of rapid industrialization and urbanization, we need a more complete urban planning system. It is very important to build a 3-D model of a city, such as disaster management, military operations, building mapping and cadastral data update. Due to the continuous population growth in urban areas in developing countries, a systematic urban planning model is very much needed. Many urban planning experts believe that the 3-D scanning created by the LiDAR system can bring more efficient development in urban planning. In the design of road systems, LiDAR pre-measurement of the surface environment can facilitate street design and calculation workload. In other words, the restrictions of population and other key factors, for reasonable urban density and optimization, need to be combined with the implementation of this technology.

1.3.4　Autonomous vehicles

Road safety is an issue that everyone is very concerned about. Advanced driver assistance systems (ADAS) can avoid traffic accidents by predicting road conditions. Therefore, cars need to be equipped with reliable on-board LiDAR systems to detect and take preventive actions, as shown in Fig. 1.8. Compared with RADAR systems for vehicles, LiDAR has very good resolution and larger field-of-view. So far, most of the automotive LiDARs use heavy and expensive motor-driven scanning mirrors, which are characterized by scanning speeds much lower than 50Hz. This speed is difficult to have further applications[27]. Use LiDAR's rotating beam for car detection and obstacle detection. The point cloud map provides the necessary data for the autonomous driving computer and indicates the potential hazards and obstacles in the environment[14].
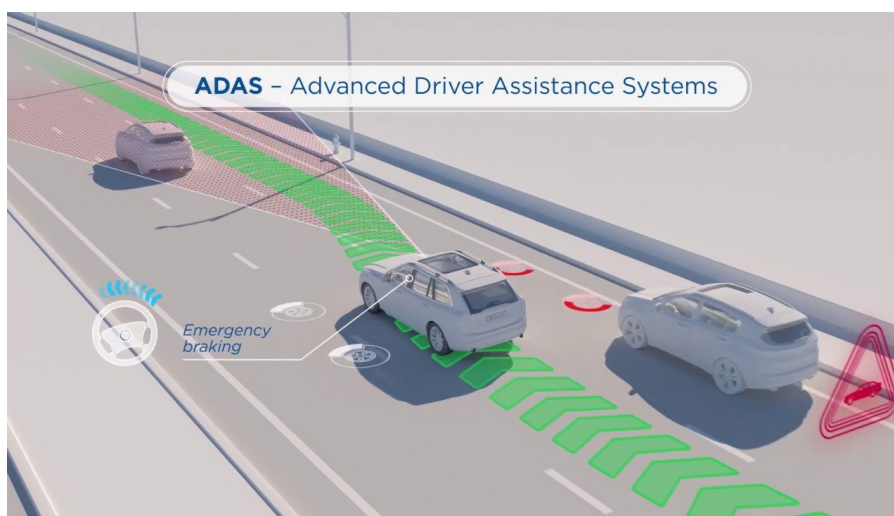
Fig. 1.8　The figure above is a schematic diagram of ADAS. Using the ADAS system can make road traffic safer.[40]

LiDAR for automobiles must balance the cost of production and the accuracy of laser scanning. This system can be installed on small cars, luxury cars and commercial trucks. Therefore, LiDAR for automobiles increasingly relies on the technology of MEMS scanners. It is hoped that through the mass-produced MEMS scanner, LiDAR for vehicles can simultaneously lower the price and scan accurately. MEMS scanner is manufactured using semiconductor technology. Using this method, a large number of components can be produced on wafers[27]. Therefore, it can be produced very efficiently. Because the MEMS scanner does not need to use mechanical bearings, it can vibrate at very high speed. MEMS scanner can reach large deflection angles at high scan frequencies of several kHz. At the same time, because MEMS scanner can scan accurately and its manufacturing cost is low[11, 28], it has great development potential in ADAS systems.

Fig. 1.9   The figure is a schematic diagram of LiDAR for vehicles. Through LiDAR, the car can detect the dynamic situation of the surrounding environment.[41]

As shown in Fig. 1.10, many manufacturers have invested in the field of autonomous driving LiDAR. If we classify its scanning method and the type of laser light source, the following comparison chart can be obtained.
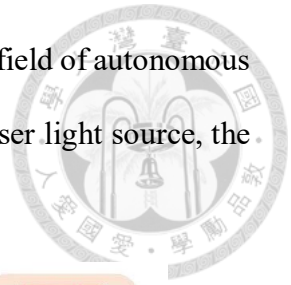
Fig. 1.10 Manufacturers of LiDAR for vehicles on the market are classified according to their scanning methods and laser light sources.[42]

Chapter 2   Principle of LiDAR

2.1   LiDAR architecture overview

LiDAR systems used in autonomous vehicles are a rapidly growing market. Due to the active activities in this field, this chapter will discuss the basic details of currently used technologies and components, rather than comparing and analyzing different applications of LiDAR. First, the technology of laser ranging will be introduced, and then the method of transition from single-point LiDAR to three-dimensional measurement covering the entire field-of-view (FOV) will be introduced. Finally, we will introduce the light sources and photodetectors currently in use.

2.1.1   Single point detection

Pulsed TOF techniques are the most typical laser ranging techniques. The principle is to use the time required for the light pulse in the medium to travel to the target to infer the distance. As shown in Fig. 2.1, the pulsed laser light is emitted after passing through the collimating lens and reflected by the target back to the receiver. In addition to receiving the reflected signal, the receiver also receives the signal emitted by the light source. After calculating the time difference between the two, the distance between the light source and the target can be obtained[4].
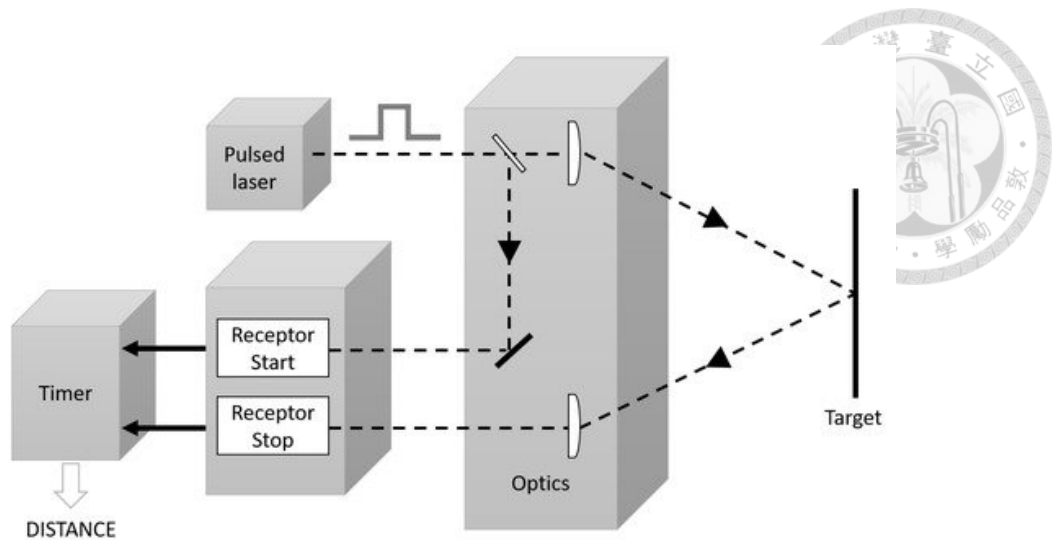
17

Fig. 2.1   The pulsed laser light is emitted after passing through the collimating lens and reflected by the target back to the receiver.[2]

The achievable resolution (ΔR_{min}) within the range is directly proportional to the available timing resolution (Δt_{min}). As a result, the resolution in the depth measurement is converted to the resolution in the timing electronics. The typical resolution value of the time interval measurement can be preset within the range of 0.1 ns to obtain a resolution of 1.5 cm depth[2]. Such a value can be considered as the current reference, limited by errors and noise in the time electronics. The resolution can be significantly improved by using statistical information, and several pulses per data point are required, which reduces the performance of the sensor in key aspects such as frame rate or spatial resolution.

In theory, the maximum reachable range (R_{max}) is only limited by the maximum time interval (t_{max}) that can be measured by a timer. In fact, this time interval is large enough, so the maximum range will be limited by other factors. In particular, the loss of laser energy in the propagation process (especially in the diffuse target), coupled with the high bandwidth of the detection circuit (noise and interference that bring noise), creates a competition between weak return signals and electronic noise. Thus , the signal-signal-

to-noise ratio (SNR) is the limiting factor in the actual range of pulsed lidar[10]. Regarding the maximum range, the alignment to be considered is the ambiguity distance (the maximum range that can be measured clearly). In the pulse approach, it is limited by the simultaneous presence of multiple pulses in flight, so the speed of the laser is related to pulse repetition.

2.1.2　Image strategies

The previous chapter explained how to measure the distance of a single point. But what people are interested in is getting a 3-D point cloud image. In order to measure the data of each point in the space, many methods have been proposed. Each scanning architecture will be explained in detail in section 2.2.

2.1.3　Light source

Lidar usually uses laser sources with wavelengths ranging from the infrared region (usually 0.80 to 1.55μm) to use the atmosphere as a transmission medium, and these beams are invisible to the human eye. The light source is mainly used in three areas: 0.8μm to 0.95μm band, controlled by a diode laser that can be combined with Si-based photodetectors, 1.06μm lasers can still be used for Si detectors, usually based on fiber lasers, and 1.55μm laser, which can be purchased from the telecommunications industry, requires an InGaAs detector[2]. However, because the detection principle of lidar is universal, other wavelengths are also possible, and can work in most cases, regardless of the selected wavelength. Usually cost and eye safety should be considered when choosing the wavelength. For example, 1.55μm can provide more power within the eye safety limit defined by Class 1, but if the detector needs to be larger than the conventional

19

telecommunications scale (200μm), it may become very expensive.

Fiber lasers use fiber as the active medium of the laser. The optical fiber is doped with rare earth elements (such as Er^{3+}) and pumped by one or more optical fiber coupled DL. In order to turn the fiber into a laser cavity, some type of reflector (mirror) is needed to form a linear resonator or build a fiber ring structure (as shown in Fig. 2.2).
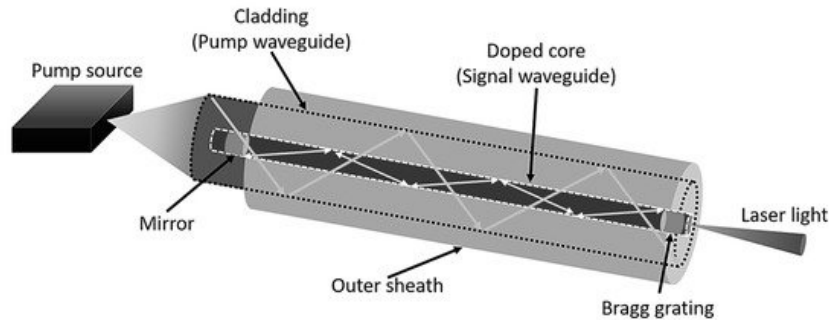
Fig. 2.2   Schematic diagram of Fiber laser.[2]

Fiber lasers can have a long active area, so they can provide high optical gain. Currently, there is a high-power fiber laser whose output power of a single fiber is hundreds of watts, sometimes even several kilowatts (up to 100 kW in continuous wave operation). There are two main reasons for this potential: On the one hand, the surface area/volume ratio is high, because the temperature rise is low and the distribution is uniform, so it can be effectively cooled; on the other hand, the guiding effect of the fiber is avoided even under obvious heating conditions The thermo-optical problem is solved. The waveguide properties of the fiber also allow the generation of diffraction-limited spots, that is, the smallest possible spot due to the laws of physics. The beam quality is very good, so the introduced beam divergence is very small, which is only related to the numerical aperture of the fiber. Usually kept within 0.1 degrees. This divergence is proportional to the coverage area of the beam on the target and is therefore directly related to the spatial resolution of the lidar image.

Diode laser is very advantageous in the application of LiDAR. Because Diode laser is cheap and compact, it meets the needs of autonomous driving LiDAR. Although Diode laser provides less power than optical fiber, it is sufficient for autonomous driving systems. When the Diode laser beam is launched, the horizontal and vertical divergence angles are different, which greatly affects the distance and accuracy of LiDAR. In order to design a Diode laser light source suitable for LiDAR systems, it must be collimated. Make the divergence angle of the laser beam as small as possible and the spot on the surface of the receiving object as small as possible. The following table compares the characteristics of different types of lasers.
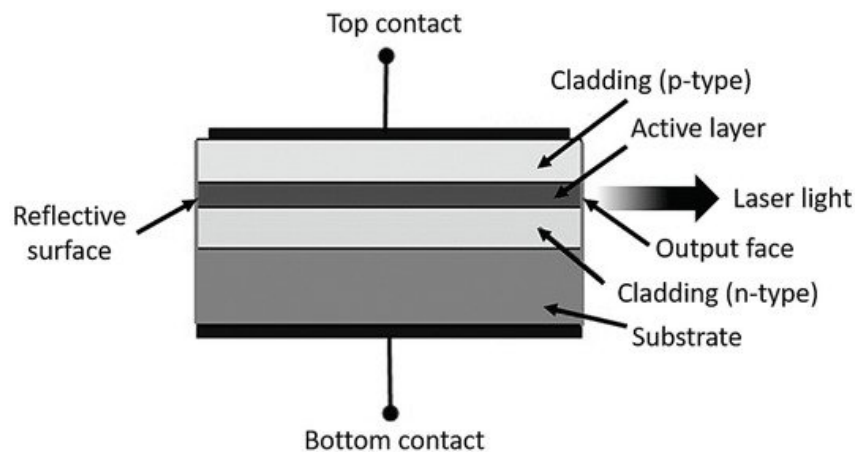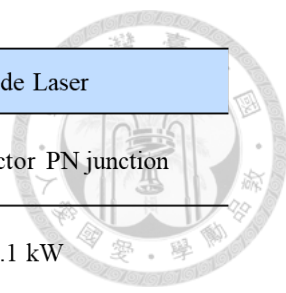
Fig. 2.3   Schematic diagram of a diode laser.[2]
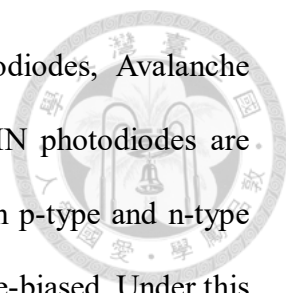
	Fiber Laser	Diode Laser
Amplifying media	Doped optical fiber	Semiconductor PN junction
Peak power (typ)	>10 kW	0.1 kW
Pulse width	<5 ns	100 ns
PRR	<1 MHz	~100 ns
Main advantage	Pulse peak power, beam quality	Cost, compact
Main disadvantage	Cost	Max output power and PRR. Beam quality

Table 2.1 LiDAR sources main features.

2.1.4 Photodetectors
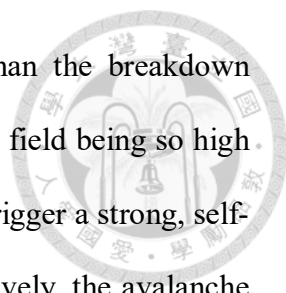
In addition to the light source, the photodetector is an important component with specialized functions in LiDAR. Photodetectors are devices that receive the bounce signal of laser light and can be used for ToF measurement. It must have both great sensitivity and the ability to measure short pulses. The raw material of Photodetectors directly affects the wavelength of light that it can detect. Currently , Si-based detectors are used between $0.3\mu m$ and $1.1\mu m$, while InGaAs detectors are used for sections above $1.1\mu m$, but have a sensitivity of $0.7\mu m$ or even higher[29]. InP detectors and InGaAs/InP heterostructures have also been considered to be able to utilize mid-infrared detectors, although they are rarely used in commercial lidar systems because they are costly if they exceed telecommunication standards and eventually require cooling to reduce noise figures. The Time-Correlated Single Photon Counting (TCSPC) technology uses the time distribution of the received pulses to obtain statistical measurements of the waveform of the signal over time[9, 30].

Photodetectors used for LiDAR mainly include PIN photodiodes, Avalanche photodiodes, and Single-photon avalanche photodiodes[19, 31]. PIN photodiodes are diodes with a wide undoped intrinsic semiconductor region between p-type and n-type doped regions. When used as a photodetector, the PIN diode is reverse-biased. Under this condition the diode is not a conductor, but when a photon with enough energy enters the depletion region it creates an electron-hole pair. The field of the reverse bias then sweeps the carriers out of the region creating a current proportional to the number of incoming photons. This gives rise to a photocurrent sent to an external amplification circuit. The depletion region stays completely within the intrinsic region, and it is much larger than in a PN diode and almost constant-sized, regardless of the reverse bias applied to the diode. In LiDAR imaging systems, PIN photodiodes are usually used as detectors to detect laser pulses as the starting signal for TCSPC conversion[2].

An avalanche photodiode (APD) is a diode-based photodetector that has a relatively high reverse bias voltage through an internal gain mechanism to detect external photoelectric signals. Under high bias voltage, a strong internal electric field is generated, which then generates carriers and generates additional secondary electrons. Because the process of learning avalanche of electrons occurs within a distance of several microns, it can produce a very high gain factor[8, 32]. APD is a very sensitive detector, so only a very weak photon signal can be activated[20]. However, the APD will produce current fluctuations in the avalanche process, thereby producing fluctuations in the SNR, which offsets the advantage of the SNR gain. Generally speaking, the performance of APD is much better than PIN photodiodes. Because APD has a larger detection wavelength range and can detect weak light, it can be used in various applications that require high sensitivity.

APDs working in Geiger-mode are known as single-photon avalanche diodes

23

(SPADs)[15]. The working voltage of SPAD is slightly higher than the breakdown threshold voltage. Because the electric field is very high, the electric field being so high that a single electron–hole pair injected into the depletion layer can trigger a strong, self-sustained avalanche. In order for the Geiger mode to operate effectively, the avalanche process must be stopped, so the photoelectric The detector returns to its original static state. Once the photocurrent is triggered, the circuit reduces the voltage on the photodiode below the breakdown voltage in a short time, thereby stopping the avalanche. After a period of recovery, the detector will regain its sensitivity and be ready to receive other photons. SPAD is very effective in low-light detection and can be used when extremely high sensitivity of the single-photon detection level is required. From low-light biomedical imaging to applications of quantum optics. Devices with optimized amplifier electronics are also available in CMOS integrated form, and can even be used as a large detector array. With TCSPC technology, it is possible to obtain statistical measurement results of the waveform of the signal over time by measuring the time distribution of the received pulse, thereby designing a LiDAR system. Their main drawback is their sensitivity to large back reflections which may saturate the detector and leave it inoperative for short periods, an event easily found in real life where large retroreflective signs are present almost everywhere on the road as traffic signs.

As shown in Fig. 2.4, the I-V curve of different photodetectors, showing the different behaviour of gain. Each different photodetector has its own characteristics. Table 2.2 shows the main characteristics of each photodetector.
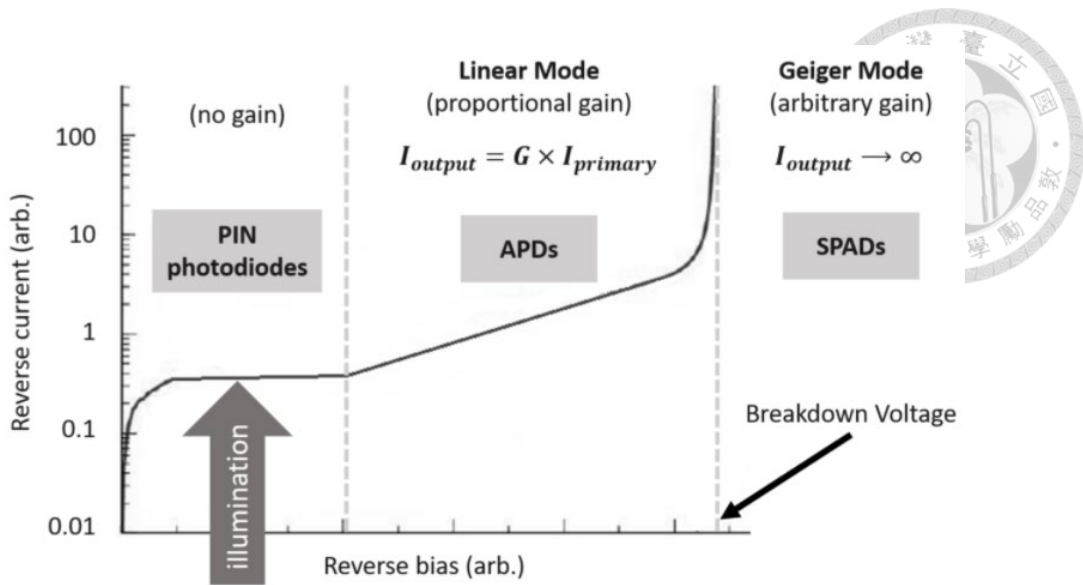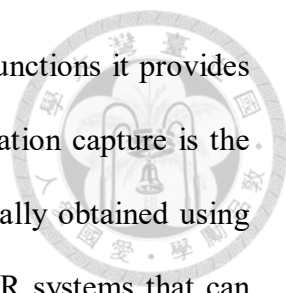
Fig. 2.4   I-V curve diagram of different photodetectors, showing the different behaviour of gain.[2]

	PIN	APDs	SPADs
Gain	1	Linear	Geiger
Main advantage	Fast	Adjustable gain by bias	Single photon detection
Main disadvantage	Limited for low SNR	Limited gain	Recovery time

Table 2.2 Each different photodetector has its own characteristics. This table compares the main characteristics of each photodetector.

2.2   Beam deflection mechanisms

The classification of LiDAR instruments may be broad and subjective, and there are many classification methods because of different application environments. Nevertheless,

25

the instrument usually uses the three types of information capture functions it provides for classification, namely time, spectrum and space. Spatial information capture is the basic function of every LiDAR instrument. This information is usually obtained using time-of-flight (TOF) measurements. There are three types of LiDAR systems that can collect spatial information: one-dimensional (1D), two-dimensional (2D), and three-dimensional (3D). With the help of optical technology to extend the scanning range of LiDAR 1D, 2D and 3D spatial information can be collected. Spatial information is essential for constructing accurate 3D maps of the environment. With the increasing demand for LiDAR in the market, many different laser beam scanning mechanisms have recently been developed. From the scanning method to classify, LiDAR can be divided into four categories. They are Non-scanning LiDAR, OPA scanners, Motorized optomechanical scanner, and MEMS scanner. Because LiDAR is composed of many subsystems, such as power supply, ranging module, control system, optical lens, etc. Chapter 2.2 will classify the different laser scanning systems and introduce each system in detail.

A fully functional LiDAR system will consist of four main subsystems, including power management, laser rangefinder, beam deflection, and master controller units[1]. These basic modules are indispensable. Fig. 2.5 illustrates the operational relationship between the various modules. If one of these parts is missing, LiDAR will lose some of its functions. Therefore, failures in any of these subsystems may cause the LiDAR system to lose function. However, in the absence of a beam deflection rotor system, LiDAR can still be used as a one-dimensional LiDAR, usually called laser rangefinder (LRF).
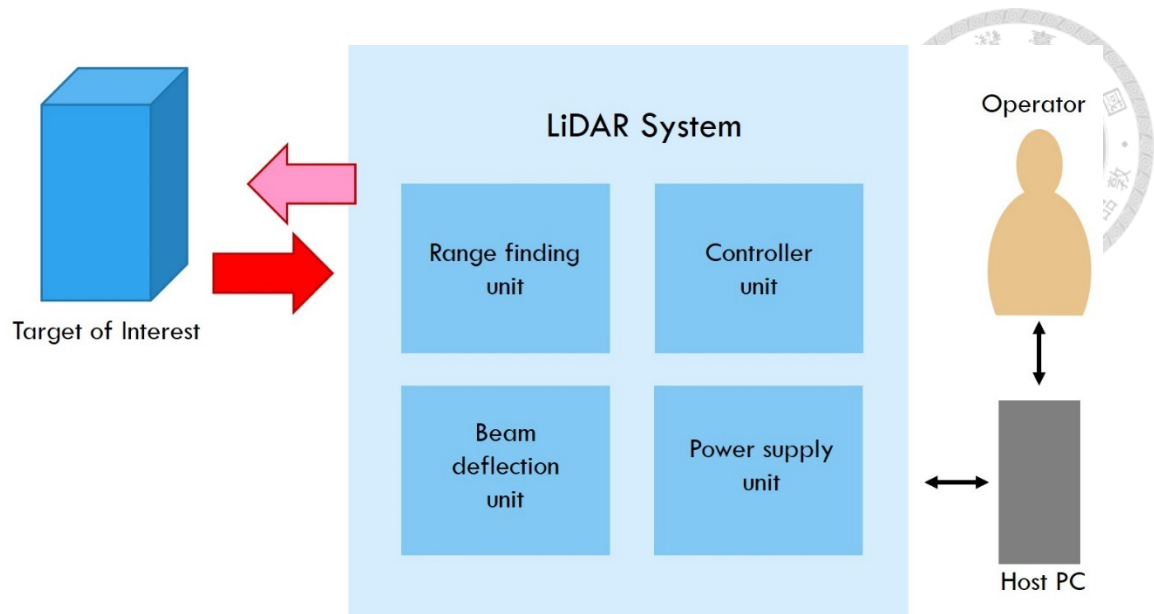
Fig. 2.5   A fully functional LiDAR system is made of four major subsystems namely

laser rangefinder, beam deflection, power management, and master controller units.

As mentioned earlier, LiDAR instruments without beam deflection systems are usually called LRF. At this time, LiDAR can only collect 1D distance data. This instrument is only suitable for collecting distance information from one point to another. In order to obtain 2D or 3D spatial information from the environment, the laser beam transmitted by the LRF must be deflected so that the laser beam can scan the entire space. There are several beam deflection mechanisms used (often called scanning methods). They are roughly divided into four categories: Non-scanning LiDAR, OPA scanners, Motorized optomechanical scanner and MEMS scanner. As shown in Fig. 2.6. In the following sections, each beam deflection method will be discussed in detail.

27
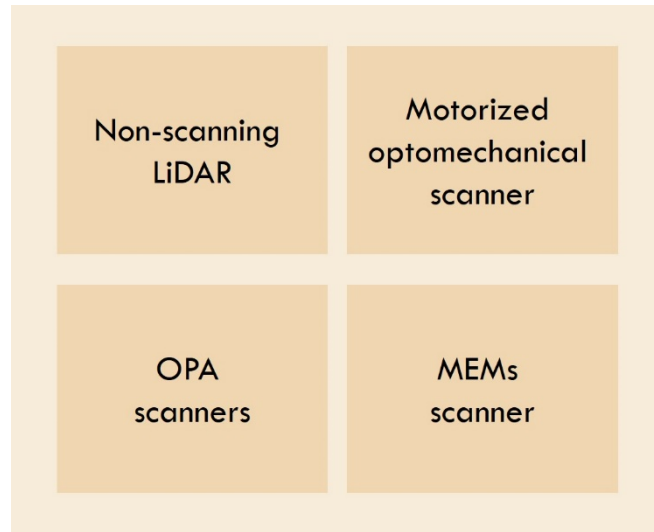
Fig. 2.6   Classification of scanning mechanism for LiDAR systems.

2.2.1   Non-scanning LiDAR

Non-scanning LiDAR is also called Flash LiDAR. "Flash" refers to the optical characteristics of this system. The area to be detected is completely illuminated with laser light, just like a camera with a flash. A series of photodetectors on the image plane simultaneously pick up the time-of-flight (ToF) 2D FoV, as shown in Fig. 2.7. All parts of Flash LiDAR are solid components, and its advantage is that there are no moving parts. Therefore, Flash LiDAR has the advantages of anti-vibration, compact size and low price. The resolution of non-scanning LiDAR based on the detector array is limited by the size and density of the detector array. In addition, illuminating the entire FOV with laser light means that each pixel of the photodetector array receives only a small portion of the return laser power, resulting in a very low signal-to-noise ratio (SNR) value. This feature greatly limits the distance measurement range or requires very high laser power.
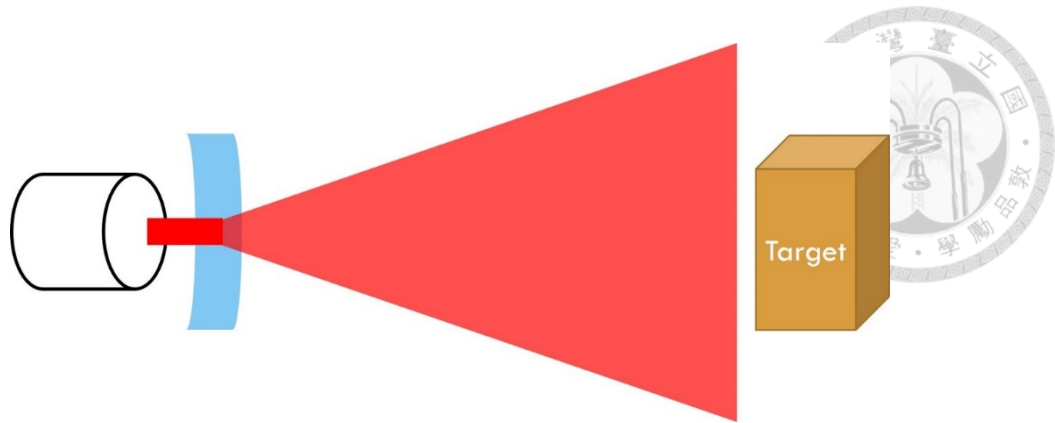
Fig. 2.7   Flash LiDAR illuminates the area to be detected with laser light, just like a
camera with a flash.

Flash LiDAR covers the scene with light so that the illuminated area matches the detector's field of view. As shown in Fig. 2.8, flash LiDAR illuminates the entire object space with light, while scanning LiDAR scans each point in the space independently. Vertical cavity surface emitting lasers (VCSELs) make it possible to simultaneously emit thousands of beams in different directions. The APD array on the detection optical focal plane is the detector. Each APD measures ToF independently to achieve the APD imaging the target characteristics. This is a true "no moving parts" method, where the tangential resolution is limited by the pixel size of the 2D detector.

However, the main disadvantage of Flash area array LiDAR is the light intensity of the reflected photons. Once the distance exceeds several tens of meters, the number of returned photons is too small for reliable detection at all. If the scene is not covered by light, at the expense of tangential resolution, using grid point structured light for illumination, this can be improved.
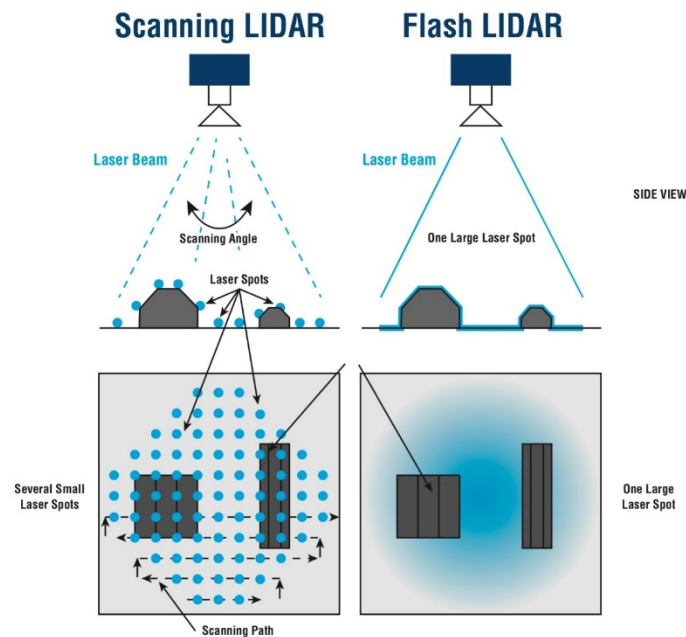
Fig. 2.8　Flash LiDAR illuminates the entire detection object space with light, while scanning LiDAR scans each point in the space independently. Although the flash LiDAR has a simple structure and low cost, it is limited by the pixel size of the 2D receiving element, and the resolution is poor.[43]

2.2.2　OPA scanners

Optical phased array (OPA) scanners can control laser beams. They have a higher signal-to-noise ratio (SNR) advantage than Flash LiDAR, so they are more popular and more mature. The phased array transmitter is composed of several transmitting and receiving units. By changing the voltage loaded on different units, the characteristics of the light waves emitted by different units (such as light intensity and phase) are changed to achieve independent control of the light waves of each unit, as shown in Fig. 2.9. By adjusting the phase relationship between the light waves radiated from each phase control unit, mutually reinforcing interference is generated in the set direction to achieve a high-

intensity beam. The light waves emitted from each unit in other directions cancel each other out, so the radiation intensity is close to zero. Under the control of the circuit system, the phase control units that make up the phased array can make the direction of one or more high-intensity light beams realize random scanning according to the designed program. OPA is a typical solid-state beam control technology that can realize non-mechanical control of the beam.
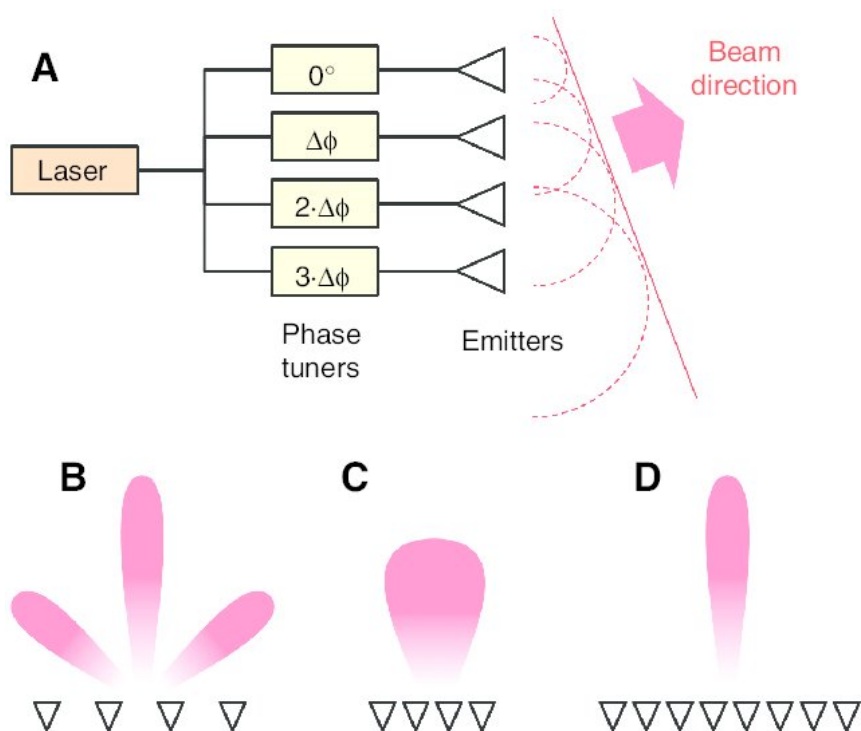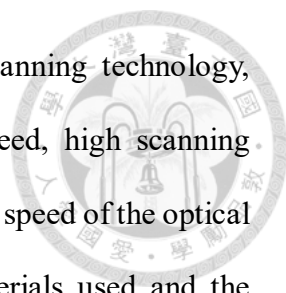
Fig. 2.9   Operation principle of phased arrays. (A) Schematic of phased array operation, showing a laser feeding an array of emitters. The phase of the output of each emitter can be tuned (yellow boxes) and is shown (dashed red circles). In the far field, these add up to a beam. The design trade-offs are shown for (B) widely spaced emitters (triangles), (C) densely spaced emitters, and (D) increasing the number of emitters. The output beam angle and amplitude are shown schematically in red in (B–D).[33]

Generally speaking, compared with traditional mechanical scanning technology, OPA scanning technology has three advantages: fast scanning speed, high scanning accuracy or pointing accuracy, and good controllability. The scanning speed of the optical phased array depends on the electronic characteristics of the materials used and the structure of the device, and generally can reach the order of MHz. So the scanning speed of OPA LiDAR is very fast. The scanning accuracy of the optical phased array depends on the accuracy of the control electrical signal (usually a voltage signal), which can be in the order of μrad (one thousandth of a degree) or more. Therefore, the scanning accuracy or pointing accuracy is high and the controllability is good. The beam pointing of the optical phased array is completely controlled by electrical signals, and it can be pointed arbitrarily within the allowable angle range. It can perform high-density scanning in the target area of interest and sparse scanning in other areas, which is suitable for autonomous driving environments Perception is very useful. However, OPA LiDAR is difficult to process and the manufacturing process is difficult. The optical phased array requires that the size of the array element must not be greater than half a wavelength. Generally, the current working wavelength of the laser radar is about 1 micron, which means that the size of the array element must be no greater than 500 nanometers. Moreover, the larger the number of arrays, the smaller the size of the array unit, and the energy is concentrated toward the main lobe, which requires higher processing accuracy. Fig. 2.10 is a schematic diagram of the working principle of the Solid State LiDAR S3 optical phased array scanning radar disclosed by Quanergy. It can be seen that S3 uses optical phased array technology to achieve laser scanning. The principle is the same as that of phased array radar. The laser beam angle can be changed by adjusting the phase difference of each transmitting unit in the transmitting array.

32
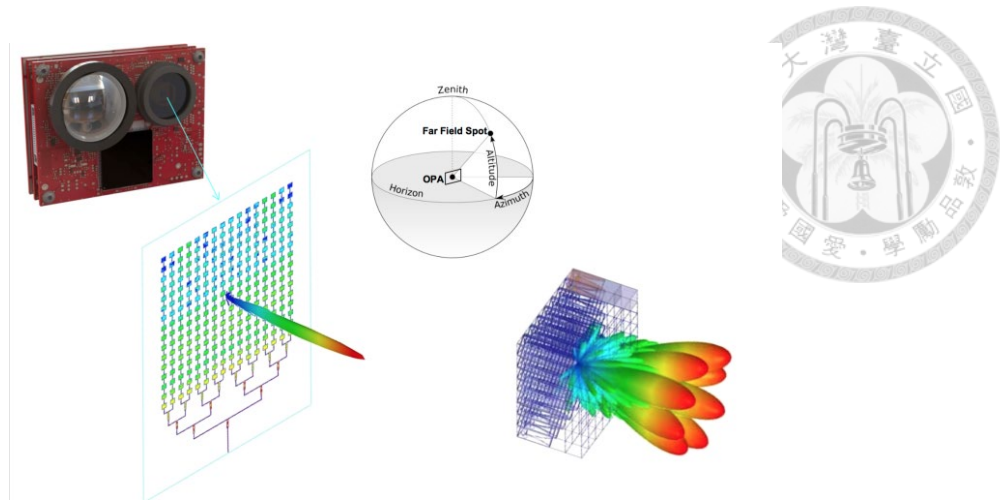
Fig. 2.10 A schematic diagram of the working principle of the Solid State LiDAR S3

optical phased array scanning radar disclosed by Quanergy. The principle of OPA

LiDAR is the same as that of phased array radar. It changes the angle of laser emission

by adjusting the phase difference of each transmitting unit in the transmitting array.[44]

2.2.3   Motorized optomechanical scanner

Motorized optomechanical scanner is the most common type of LiDAR scanner. As

shown in Fig. 2.11. LiDAR based on a rotating motor turns into a 2D scanner by installing

1D LiDAR on a rotating platform. By installing the 2D scanner on the rotating platform

in the second direction, a 3D scanning system is formed.
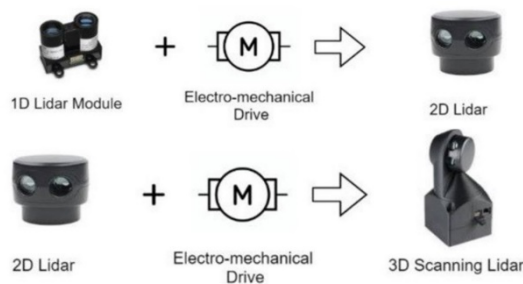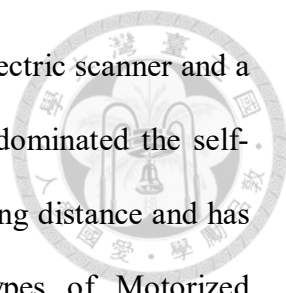
Fig. 2.11 The design concept of LiDAR system based on rotating motor. Rotary motor

LiDAR is a 2D scanner by installing 1D LiDAR on a rotating platform. By installing

the 2D scanner on the rotating platform in the second direction, a 3D scanning system is

formed.[3]

In 2007, Velodyne released the first 64-line lidar based on an electric scanner and a bunch of multiple lasers and photodetectors. This technology has dominated the self-driving car market. Since this type of scanner can use a longer ranging distance and has a wider FoV, it has many applications. There are several types of Motorized optomechanical scanners. The most common one is to stack multiple transmitter and receiver channels vertically and rotate by a motor to produce a full 360°FoV with multiple horizontal lines, as shown in Fig. 2.12. The received signal and power must be wirelessly transmitted from the rotating part to the substrate. This kind of lidar is not efficient and is susceptible to mechanical shock and wear. In addition, their vertical resolution is fixed and depends on the number of transmitter and receiver channels, so high vertical resolution always comes at the cost of high cost. And because the scanning speed is slow, it is more difficult to scan fast-moving objects, so it is difficult to use in automatic driving systems. In addition, most of the motorized scanning LiDARs available on the market target geological surveys. With the development of autonomous vehicles, especially unmanned aircraft (UAV), the market and demand for compact LiDAR are rapidly expanding[25]. However, current LiDAR solutions based on electric scanners have poor performance, are also very expensive, bulky and consume power[22, 34]. For example, the challenge for driverless cars is that LiDAR technology is expensive. Currently, the cost of LiDAR devices suitable for driverless cars is as high as $80,000, making it the most expensive component in driverless cars.
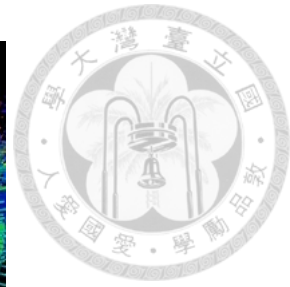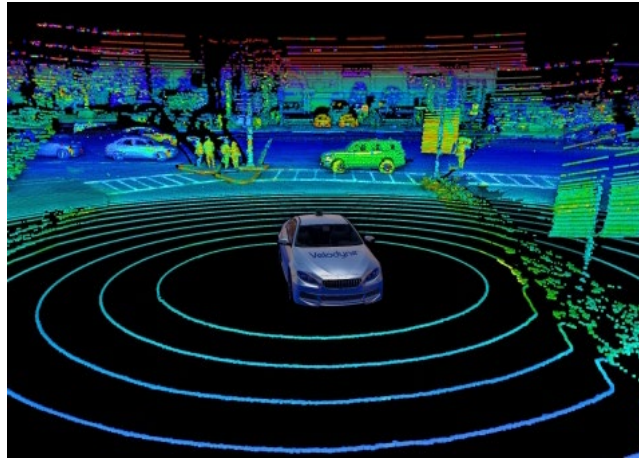
Fig. 2.12 Motorized optomechanical scanner produced by Velodyne. Although the rotating motor can provide a clear point cloud image, the expensive manufacturing cost and slow scanning speed make it difficult for the Motorized optomechanical scanner to be practically applied to the automatic driving system.[45]

2.2.4 MEMS scanner

As mentioned in the previous chapter, both OPA LiDAR and Motorized optomechanical scanner LiDAR must overcome many major obstacles before they can be actually used in autonomous vehicles. Fortunately, Micro-Electro-Mechanical Systems (MEMS) technology provides a viable alternative. MEMS mirrors have achieved great commercial success in fiber optic communications, projectors and displays[27, 35, 36]. MEMS mirrors can steer, modulate, and switch light, as well as control phase. The most critical feature of MEMS mirrors is that they are small and can guide light in free space. Therefore, compared with Motorized optomechanical scanner, MEMS scanner is superior in cost, size and scanning speed. In the LiDAR solution based on MEMS mirrors, only the tiny mirror plate of the MEMS device (with a diameter in the range of about 1–7 mm) moves, while the rest of the components in the system remain stationary. Therefore, MEMS LiDAR is usually called quasi-static-state LiDAR, which is the ultimate

compromise between solid-state LiDAR and mechanical LiDAR.
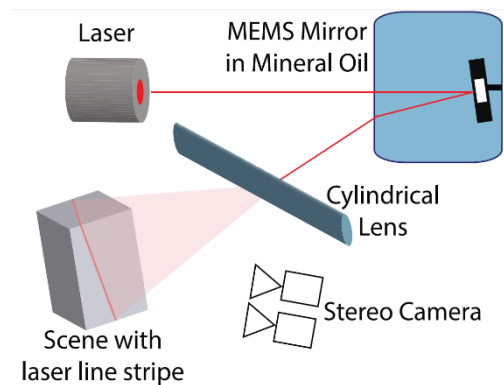
Fig. 2.13 The structured light camera design uses a one-dimensional MEMS mirror and

scattered laser light.[37]

Three-dimensional lidar can be constructed with 1D MEMS mirrors and diffuse laser

beams, as shown in Fig. 2.13. The horizontal scanning beam from the MEMS mirror

diffuses to the laser line through the diffuser lens. Therefore, the scanning beam can cover

the vertical and horizontal directions. The horizontal resolution in pixels depends on the

measurement sampling rate and the scanning frequency of the MEMS mirror. As shown

in Fig. 2.13, the structured light camera design uses a one-dimensional MEMS mirror and

scattered laser light. Another common problem with this LiDAR is the short maximum

detection distance. The first reason is that the power of the laser is distributed in a line,

resulting in low optical power density.

Another similar architecture uses an array of laser sources to form vertical scan lines,

a 1D MEMS mirror to scan the vertical lines in the horizontal direction, and a 2D PD

array to collect optical signals from the target. As shown in Fig. 2.14. This architecture

can partially solve the problems of low laser power density and low signal-to-noise ratio

of detection signals, and is a step towards realizing commercial lidar for autonomous

driving. However, additional alignment and assembly work is required to align multiple

36

lasers with the MEMS mirror plate. Because each scan is a 1D scan of the target, its resolution depends on the size of the detector's pixels. The potential problems of laser collimation with such small MEMS mirrors may result in poor angular resolution of LiDAR.
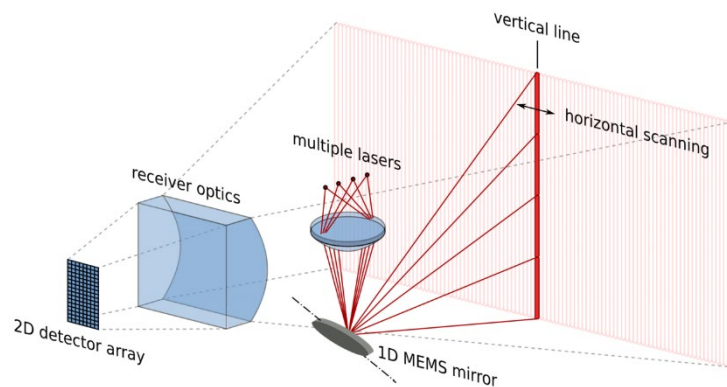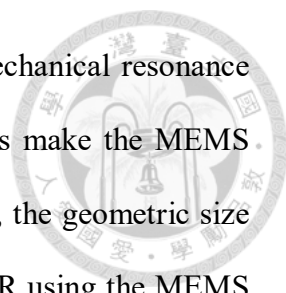
Fig. 2.14 The LiDAR designed by Infineon uses a 1D MEMS mirror and a lasers array. It uses an array of laser sources to form vertical scan lines, a 1D MEMS mirror to scan the vertical lines in the horizontal direction, and a 2D PD array to collect optical signals from the target.[46]

Traditional scanning imaging LiDAR systems generally use double pendulum mirrors, double galvanometers and rotating polyhedral reflecting prisms. The scanning system composed of these macroscopic optical elements is bulky and heavy. Using MEMS technology, a very compact micro scanning mirror can be directly integrated on a silicon-based chip, and the light of the laser can be reflected by the MEMS scanning mirror, thereby achieving micron-level motion scanning. With this technology, no mechanical rotating parts in LiDAR can be seen macroscopically.
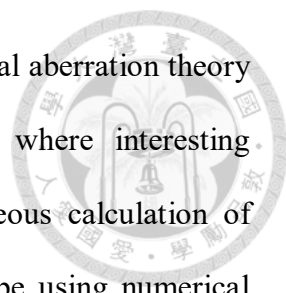
The way to make the scanning LiDAR more compact is to use MEMS micro-mirrors to control the beam deflection direction in the 2D direction with MEMS mirror. Although there are still some moving parts technically (the micro mirror also vibrates), the vibration

37

amplitude is small and the frequency is high enough to prevent mechanical resonance between the MEMS micro mirror and the car. These characteristics make the MEMS LiDAR structure more reliable and easier to manufacture. However, the geometric size of the MEMS mirror limits its scanning angle, so the FOV of LiDAR using the MEMS mirror is limited. But because of its low cost, high reliability and fast scanning speed, MEMS LiDAR has great potential in the development of LiDAR technology. This paper focuses on the design of a large-angle MEMS LiDAR system. By combining free-form surface optics and a laser scanning system, the MEMS LiDAR scan angle is too small. The wide-angle optical lens will be discussed in detail in Section 3.4.

2.3 Wide angle scanning lens

When designing the wide-angle lens in front of the MEMS mirror, because the scanning angle needs to be magnified very many times, the resulting aberration may become very large. Therefore, the method of designing a wide-angle scanning mirror is very important. In recent years, because of the popularity of computer-aided computing, we can design optical lenses with more complex surface structures. Free-form optical devices involve the design of optical elements that have at least one surface that is not translationally or rotationally symmetric with respect to the propagation axis. This topic is becoming more and more popular in the optics world, partly because of the rapid development of new computing technologies and the emergence of potential applications. Generally, the design of free-form components has been combined with the theoretical approximation method of brute force optimization technology, which has been proven to be able to obtain useful results and diversity under special circumstances[47,48]. Recently, the generation of free-form mirrors has been studied [49,50], which greatly reduces

optical aberrations. Many articles [51-53] developed free-form optical aberration theory using numerical optimization schemes. Recently, several cases where interesting solutions are free-form have been reported through the simultaneous calculation of multiple surfaces. Radial based on the general Cartesian oval shape using numerical methods for symmetry has been reported [54,55]. Levi-Civita first considered the general Cartesian ellipse problem in 1900, but did not give an analytical closed-form formula [56]. The generalized Cartesian ellipse problem involves finding a refracting surface that transforms a given incident wavefront into another given outgoing wavefront. Optical system design involves the optimization of optical imaging, optical sensing and image post-processing to meet application-specific specific system parameters (for example, field of view), while also satisfying physical (for example, packaging size and weight) and cost equire constraints. In many cases, especially when a set of constraints is uncommon, it turns out that designing high-performance systems is challenging. In a wide-angle computing camera, the optical system produces an image with severe barrel distortion, and the digital system corrects this distortion to produce a linear final image. Wide-field optical systems usually image straight lines in the object as curves, which is undesirable for most biomedical imaging, machine vision, and other consumer applications. But in our ToF LiDAR system, the unit that composes the picture is the distance information of each object. If the distortion is too large, it will cause uneven distribution of information at each position in the picture, which is difficult to apply to LiDAR application that requires precise detection distance. In the following chapters, we will explain in detail the methods of expanding the scanning angle and their design principles.

2.3.1 Optical Angle Amplification System

Because the scanning angle of the MEMS mirror is very small, it can only scan a small area, so a set of lenses that can expand the scanning angle must be designed in front of it. The traditional feasible method is to add an angle expansion optical system to the scanning system, which consists of two lenses-a positive lens behind the MEMS mirror and a negative lens behind it. However, this traditional lens set has at least two disadvantages: (1) The divergence angle of the emitted light beam is too large. Although for short-distance targets, too large a laser divergence angle will not have a significant impact on scanning, but when used for targets tens of meters or hundreds of meters, the spot size of the outgoing beam will become larger. , The energy per unit area is rapidly reduced, causing the returned laser signal to be too small. The SNR is too low to be received by the detector. (2) The expanded scanning angle is limited (usually less than 50 degrees). If the FOV increases, the distortion will become very serious. Therefore, the method of designing a wide-angle lens is very important. In chapter 2.3.2, we will discuss in detail the design method of the wide-angle lens.

2.3.2 Optical design method

When designing the Optical Angle Amplification System, the given initial optimization parameters are very important, because if an initial value that is too different from the target value is given, the optimization system will not be able to find a value that can meet the design requirements after multiple iterations. Therefore, it is very important to calculate the initial value before designing the lens. When calculating the parameters of the wide-angle lens, matrix-type ray tracing calculations can be used. Light entering a lens with a ray height x and a ray angle φ starts at a point on a plane which is perpendicular to the optical axis. The parameters x' and φ' define the ray parameters after going through

the system. It is described by a 2 x 1 matrix. When the ray goes through the lens, the

refraction is described by a 2 x 2 matrix[57].
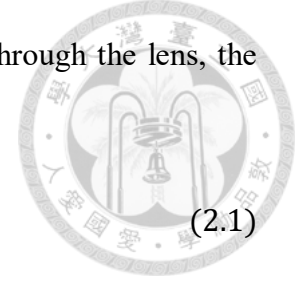
$$\begin{pmatrix} x' \\ \varphi' \end{pmatrix} = \begin{pmatrix} A & B \\ C & D \end{pmatrix} \begin{pmatrix} x \\ \varphi \end{pmatrix} \tag{2.1}$$

If there is a lateral spatial shift Δx from the optical axis or a ray angular shift ($\Delta\varphi$)

added to the to the paraxial ray, a 2 x 2 matrix is not sufficient. The theory provides an

extension for the 3 x 3 matrix. With the third component of the newly added ray vector,

the new minor axis matrix can be displayed as:

$$\begin{pmatrix} x' \\ \varphi' \\ 1 \end{pmatrix} = \begin{pmatrix} A & B & \Delta x \\ C & D & \Delta\varphi \\ 0 & 0 & 1 \end{pmatrix} \begin{pmatrix} x \\ \varphi \\ 1 \end{pmatrix} = M \begin{pmatrix} x \\ \varphi \\ 1 \end{pmatrix} \tag{2.2}$$

Using this 3 x 3 matrix, the light is converted into the local coordinate system of the

laterally moving lens, the light is traced using the ordinary lens matrix, and then the light

is converted back to the original coordinate system, thereby tracking the collimated ray

through the non-axial lens[57]. However, the calculation of the matrix is not intuitive to

us, so we integrate the concept of the matrix described above and express each field as a

vector form to calculate the starting point of design optimization. First, if the ray strikes

the input surface at the point $P(r_a, z_a)$ and emerges from the lens at $Q(r_b, z_b)$, then the

unit vectors can be express as:

$$v_1 = \frac{[r_a, (z_a - t_a)]}{\sqrt{r_a^2 + (z_a + t_a)^2}} \qquad , \quad v_2 = \frac{[r_b - r_a, z_b - z_a]}{\sqrt{(r_b - r_a)^2 + (z_b - z_a)^2}} \tag{2.3}$$

The normal unit vector of the surface pointing the incident medium can be express as:

$$n_a = \frac{[z_a', -1]}{\sqrt{1 + z_a'^2}} \qquad \text{where} \quad z_a' = \frac{dz_a}{dr_a} \tag{2.4}$$

$$n\widehat{v_2} = [\widehat{n_a} \times (-\widehat{n_a} \times \widehat{v_1}] - \widehat{n_a}\sqrt{n^2 - (\widehat{n_a} \times \widehat{v_1}) \cdot (\widehat{n_a} \times \widehat{v_1})} \tag{2.5}$$

$$\text{where} \quad n = \frac{n_2}{n_1} \tag{2.6}$$

41
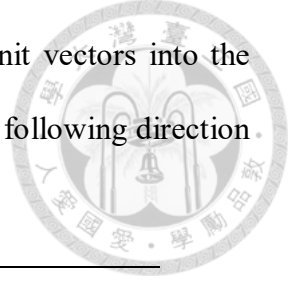
The above formula is Snell's law in vector form. Replacing the unit vectors into the Snell's law and separating the Cartesian components[58], we get the following direction of the vector v_2:

$$r_i \equiv \frac{(z_a - t_a)z_a' + r_a}{n\sqrt{z_a^2 + (t_a - z_a)^2(1 + z_a'^2)}} - z_a'\frac{\sqrt{1 - \frac{(r_a + (z_a - t_a)z_a')^2}{n^2(r_a^2 + (t_a - z_a)^2)(1 + z_a'^2)}}}{\sqrt{1 + z_a'^2}} \quad (2.7)$$

$$z_i \equiv \frac{(r_a + (z_a - t_a)z_a')z_a'}{n\sqrt{r_a^2 + (t_a - z_a)^2(1 + z_a'^2)}} + \frac{\sqrt{1 - \frac{(r_a + (z_a - t_a)z_a')^2}{n^2(r_a^2 + (t_a - z_a)^2)(1 + z_a'^2)}}}{\sqrt{1 + z_a'^2}} \quad (2.8)$$

The Fermat principle requires that both optical lengths between the point of each side of lens, O and I be the same . Thus , equating the optical paths[58], we get:

$$-t_a + nt + t_b = -\operatorname{sgn}(t_a)\sqrt{r_a^2 + (z_a - t_a)^2} + n\sqrt{(r_b - r_a)^2 + (z_b - z_a)^2}$$
$$+ \operatorname{sgn}(t_b)\sqrt{r_b^2 + (z_b - t - t_b)^2} \quad (2.9)$$

Where sng is sign function. Now we have a system of three equation. Also , we have two unknown r_b and z_b. The exact solution is given by:

$$r_b = \frac{r_i(z_b - z_a)}{z_i} + r_a \quad (2.10)$$

$$z_b = \frac{b_0 + s_1\sqrt{z_i^2[-2nf_i(z_i(z_a - t_b + t(z_i - 1)) + r_a r_i + t r_i^2 - (r_i(-z_a + t_b + t)) + r_a z_i)^2 + f_i^2 + b_1 n^2]}}{1 - n^2}$$

$$(2.11)$$

Where

$$b_0 = nf_i z_i - n^2(tz_i + z_a) + r_i^2 z_a - r_a r_i z_i + z_i^2(t + t_b) \quad (2.12)$$

$$b_1 = r_a^2 + 2r_a r_i t + (t_b - z_a)^2 + t^2(r_i^2 + (-1 + z_i)^2) - 2t(t_b - z_a)(-1 + z_i) \quad (2.13)$$

$$f_i = -sgn(t_a)\sqrt{r_a^2 + (t_a - z_a)^2} + t_a - t_b \quad (2.14)$$

42

We use a free-form optical system to design an optical system that expands the scanning angle, and propose a novel initial configuration method. In the initial configuration, each free-form surface can be calculated by mathematical expressions to calculate the corresponding surface, and then combined with the optimization function calculation in Zemax, the result of continuous iteration can produce a lens with excellent performance. The proposed multi-step design strategy can simultaneously consider the given system specifications, the relationship of the objective lens (or the magnification of the confocal system) and the generation of a real, small-distorted exit pupil with a given size. The following figure shows the flow of lens design.
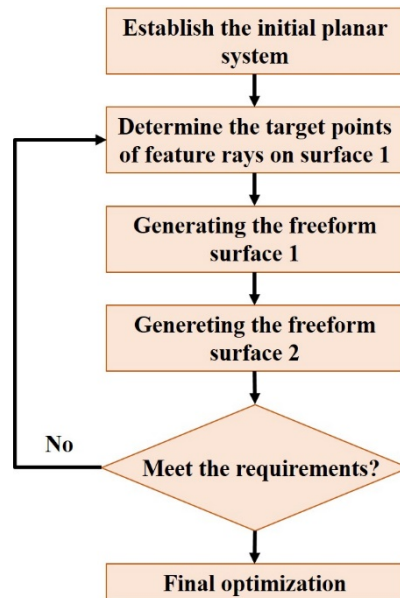
Fig. 2.15 The process of designing the lens.

Using this method, we can quickly design a lens that can meet our system requirements, and use it as a good entry configuration for further optimization of optical design software.

43

Chapter 3   Design and Simulation of the Wide-angle MEMS LiDAR System

The LiDAR system in this paper is composed of four parts: (1) Laser diode collimator is used to collimate the output light of the laser light source, (2) Laser scanning system contains MEMS mirror to deflect the laser light, (3) Wide angle scanning lens is installed in front of the MEMS mirror to enlarge the scanning angle, (4) Receiver lens design is installed in front of the receiver so that the reflected light signal at a larger angle can smoothly enter the receiver. As shown in Fig. 3.1. The light source from the laser diode is collimated by the collimator and then coupled to the MEMS mirror. After being deflected by the MEMS mirror, a small 2D scene can be scanned. However, because the deflection angle of the MEMS mirror is small, the laser scanning light cannot cover the desired scanning range, so a set of light angle scanning mirrors are designed to be installed in front of the MEMS mirror. Finally, in order to allow the optical signal of the entire scanning range to enter the receiver, a set of wide-angle receiving lenses was designed to be erected in front of the receiver. This method allows us to have a simple, lightweight and wide-angle LiDAR system.

44
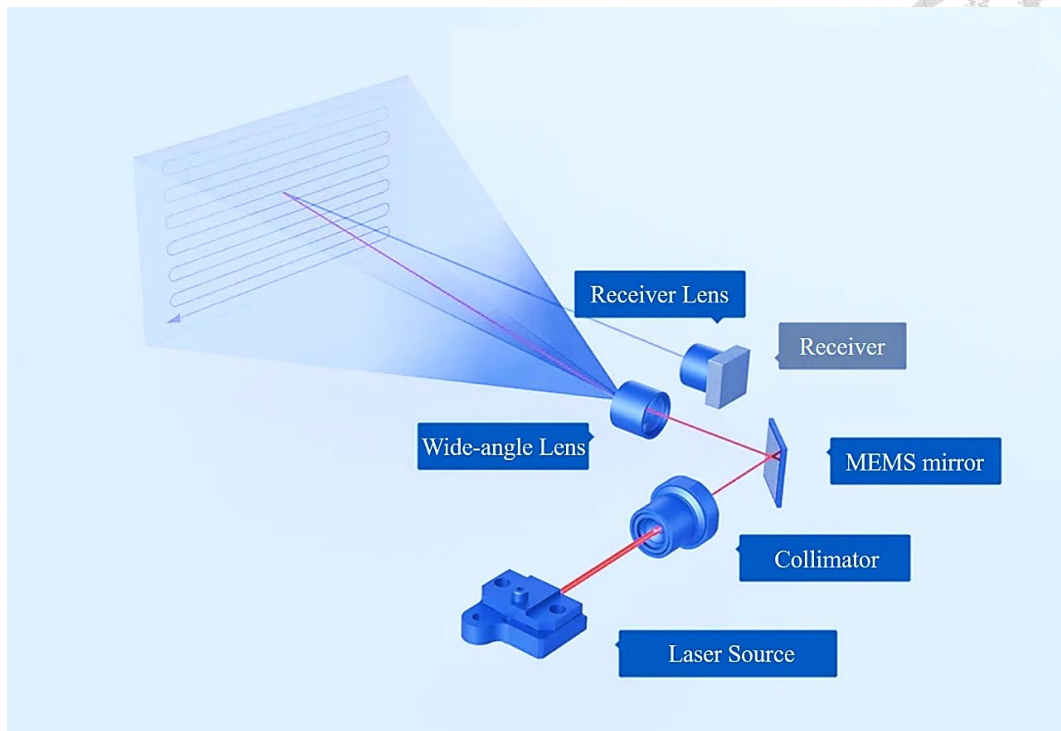
Fig. 3.1　Schematic diagram of the optical system of MEMs based wide-angle ToF

LiDAR.

The optical simulation architecture of the entire LiDAR system is shown in Fig. 3.1. The optical propagation simulation in the system is based on geometric optics theory, and the optical lens that meets the system requirements is designed. The entire system is constructed using OpticStudio® (Zemax, LLC) optical simulation software, and uses ray tracing optimization functions to make the system's optical lens quality better. In OpticStudio® (Zemax, LLC) software, you can clearly judge the pros and cons of optical lenses from many optical analyses. In Chapter 3, we will discuss the design principles and results of each optical element in the LiDAR system in sections, Chapter 3.1 will discuss the selection of LiDAR optical bands, and Chapter 3.2 will discuss the collimation methods and laser diodes. As a result, Chapter 3.3 will explain the principles used by the scanning system, Chapter 3.4 will explain the principles and results of wide-angle lens

45

design, and Chapter 3.5 will discuss the design of the receiving lens. Finally, in order to actually demonstrate the feasibility of the wide-angle LiDAR scanning system, the results of the system setup will be discussed in Chapter 4.
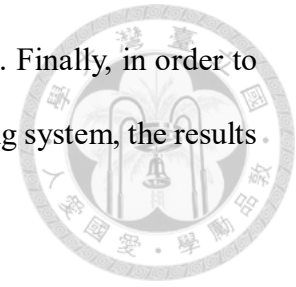
3.1　Wave length selection

Laser diodes emit light in many different wavelengths, and the most common wavelengths used in LiDAR systems are 905nm and 1550nm. However, these two different wavelengths require two completely different system architecture designs. Because 905nm is more dangerous than 1550nm, because it may harm the retina if it is not adjusted properly. The most vulnerable part of the human body to laser beam damage is the retina behind the human eye. Just staring at the sun can damage the fragile retina. This is why our eyes avoid the sun unconsciously. Since the laser is a collimated narrow beam, it is more harmful because the human eye will converge the parallel laser beam into a small spot and project it on the retina. The retina does not respond to the 905nm infrared laser currently used in automotive LiDAR, so we cannot see the laser emitted by LiDAR. However, the human eye transmits the 905nm infrared laser to the retina, so it is subject to the same legal restrictions as visible light. In fact, this will bring greater harm, because our eyes cannot instinctively avoid light sources that the retina does not respond to. However, the human eye is opaque to light with a wavelength of 1550 nm. Therefore, the light of this wavelength cannot be projected onto the retina, so that higher power LiDAR can be used without harming the human eye.

But in addition to human eye safety regulations, the cost of the receiver must also be considered. At present, a major problem hindering the development of LiDAR technology

is cost. If the cost of each part can be reduced, it will greatly help the development of LiDAR. The laser light with a wavelength of 905nm can use a silicon-based detector, which is much lower in cost than the 1550nm wavelength laser light that must use an InGaAs detector. In order to reduce costs, this paper uses a 905nm wavelength laser as the light source. At the same time, it is necessary to reduce the luminous power in accordance with human eye safety regulations, and design a more efficient optical system so that the scanning beam can detect longer distances.

3.2　Laser diode collimation

Because of its small size and light weight, laser diodes have been widely used in materials processing, laser communications, signal processing and military fields. However, due to the different dimensions of the active layer of the laser diode in the horizontal direction and the vertical direction, the divergence angle of the emitted light beam is large and uneven. This makes the laser diode's ranging distance in the LiDAR scanning process smaller than the accuracy of ranging is greatly affected. In order to ensure that LiDAR can measure the distance efficiently, the divergent beam of the laser diode must be collimated. This paper uses a cylindrical lens to collimate a 905nm laser diode. The laser beam at the receiving end is as small and uniform as possible, thereby achieving the purpose of improving the ranging distance and accuracy. We use OSRAM's laser diode model SPL UL90AT08. The divergence angle of this model laser diode in the horizontal direction is $\theta_h = 10°$, and the divergence angle in the vertical direction is $\theta_v = 25°$.

The entire collimation process can be divided into two one-dimensional problems to

47

be solved separately. Because it is necessary to collimate two laser beams with different

divergence angles, in the most basic geometric optics[57], if the light source is placed at

the focal length of the lens, the emitted beam will be parallel light. Therefore, the focal

length ratio of the two cylindrical surfaces should be similar to the divergence angle ratio

of the laser diode.

$$\frac{\theta_1}{\theta_2} = \frac{10°}{25°} = \frac{f_1}{f_2} \tag{3.1}$$

As shown in the above equation, θ_1 and θ_2 represent the divergence angles in the

vertical and horizontal directions, and f_1 and f_2 represent the focal lengths of two

cylindrical surfaces, respectively. As shown in Fig. 3.2.
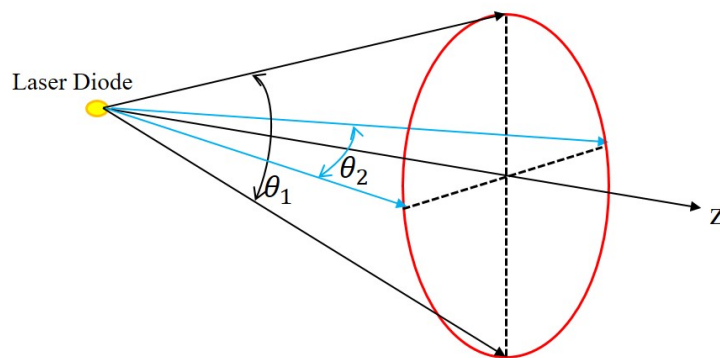
Fig. 3.2 The light emitted by the laser diode has different divergence angles in the

vertical and horizontal directions. The squares of θ_1 and θ_2 represent the divergence

angles in the vertical and horizontal directions, and f_1 and f_2 represent the focal

lengths of two cylindrical surfaces, respectively.
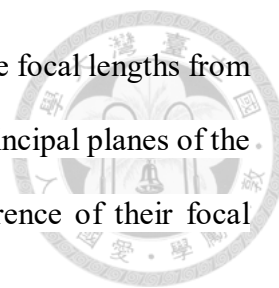
The lenses should be placed at a distance equal to their respective focal lengths from the source to create a collimated output. As shown in Fig. 3.3. The principal planes of the two lenses should be spaced at a distance apart equal to the difference of their focal lengths $f_2 - f_1$
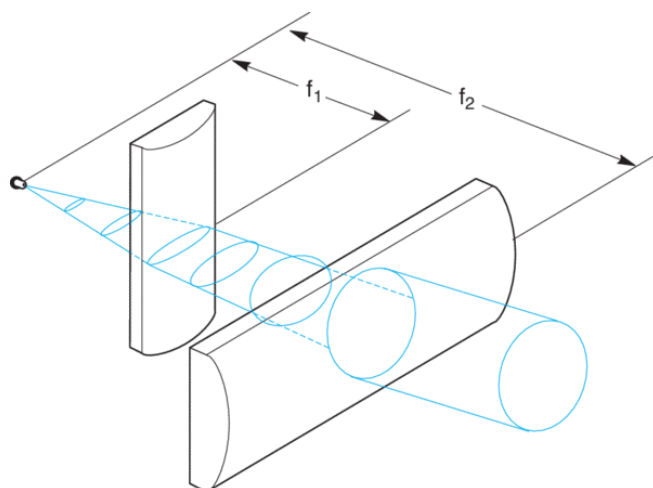
Fig. 3.3 According to the different divergence angles of the laser diode in two directions, two mutually perpendicular cylindrical surfaces are used to collimate the two directions respectively.

Then, the following equation can be derived from the geometric relationship of the lens.

$$D = 2f \left[\tan \left(\frac{\theta}{2} \right) \right]$$ (3.2)

Where D is the diameter of the outgoing beam, f is the focal length of the lens, and θ is the divergence angle of the light source. With the above equations, we can design collimators for the divergence angle of the laser diode in two different directions. As shown below.

49
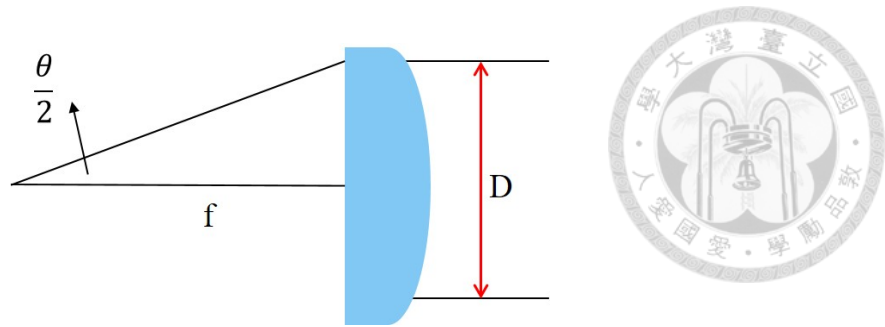
Fig. 3.4   The curve equation of the collimator can be derived from the geometric

relationship between the position of the lens and the light source. Where D is the

diameter of the outgoing beam, f is the focal length of the lens, and θ is the divergence

angle of the light source.

Using the derived equations, we designed a collimator that can collimate the laser

diode. And to calculate the placement position of the collimator.

The simulation results are shown in Fig. 3.5. In order to achieve lightweight and easy

assembly, we combine two different cylindrical surfaces on both sides of a lens, and the

two cylindrical surfaces are perpendicular to each other. In addition, in order to facilitate

processing, common PMMA is selected as the lens material. The refractive index of

PMMA is n=1.49. In this simulation, the wavelength of the laser light is 905nm.
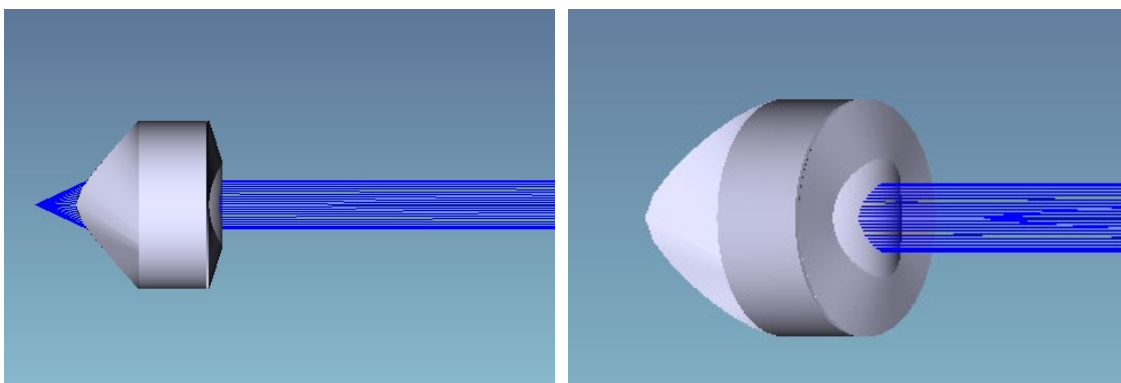
Fig. 3.5   The simulation results lay out of the collimator using Zemax.
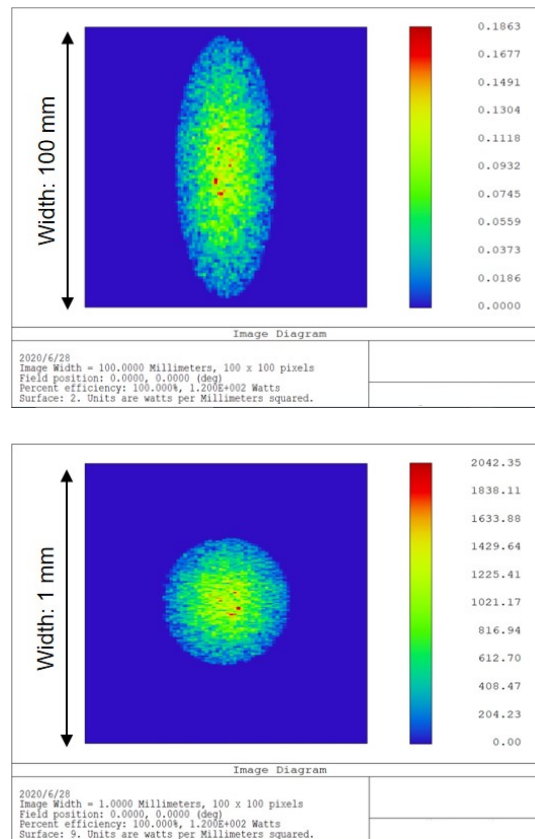
Fig. 3.6 Comparison of laser beams before and after entering the collimator. The picture above is the laser beam before entering the collimator. The picture below is the laser beam after entering the collimator. The measured distance is 100mm, the width of the diagram before collimation is 100mm, and the width of the diagram after collimation is 1mm.

As shown in the Fig. 3.6, analyze the light shift diagram before and after the laser light enters the collimator. The picture on the top is the spot map before the laser light enters the collimator. The picture on the bottom is the spot map after crossing the collimation system. Through comparison, it is obvious that the divergence angle of the beam has been greatly compressed.

As shown in Fig. 3.7, analyze the light intensity before and after the laser light enters the collimator. The horizontal axis of the light field distribution diagram represents coordinate information (unit: *mm*), and the vertical axis represents the laser incoherent

51

brightness (unit:W/cm^2) at the corresponding abscissa. The collimated laser light can meet the requirements of the LiDAR system and meet the requirements of small size and high quality.
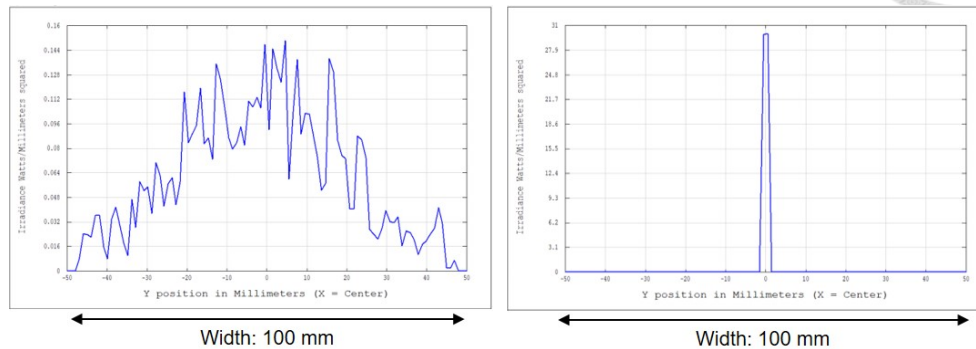
Fig. 3.7   The light intensity distribution diagram before(left) and after(right) the laser light enters the collimator. The measured distance is 100mm and the width is 100mm.

3.3   Laser scanning system

Before joining MEMS mirror, LiDAR could only scan one-dimensional spatial information, which is just a single-point laser rangefinder. After adding MEMS mirror, its vibration can make the laser scanning beam scan two-dimensional spatial information. The optical scanning device used in this research is the MEMS mirror (UM-6002G) produced by Ultimems Inc., the mirror area is 1.0×1.4 mm, and the scanning angle is ±12 degrees (fast) ±6.5 (slow) . According to the principle of geometrical optical reflection, if the incident light angle remains unchanged, the scanning angle is twice the deflection angle of the MEMS mirror, so the total scanning angle can reach 50 degrees. Because the optical signal receiving system in this study uses a wide-angle lens to receive, that is, a dual-axis architecture, there is no need to consider the returned optical signal

52

when designing the scanning system. All optical simulations are done in Zemax, as shown in the figure below. Because Zemax can only simulate a single beam in the sequence mode, the MEMS mirror obtains different deflection angles by adding many multi configurations, and then adjusts the beam travel direction when the X and Y directions are different in the multi configuration.
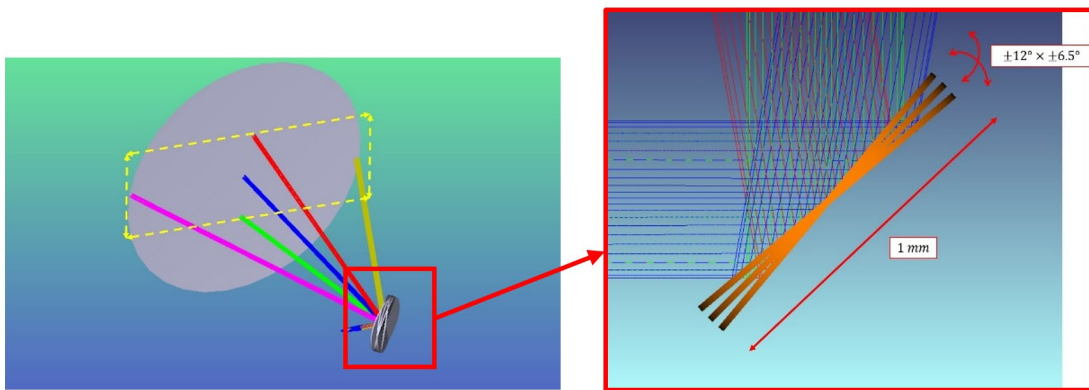
Fig. 3.8   The simulation result of the scanning system. The graph on the left shows that the collimated laser light can expand the scanning range into a two-dimensional range after passing through the MEMS mirror. The picture on the right shows the deflection of the beam after passing through the MEMS mirror.

In the system we designed, the angle between the MEMS mirror and the laser is 45 degrees, that is, the angle between the scanning area and the light source is 90 degrees. Because MEMS mirror is lighter and more responsive than other scanning systems, the system we designed can reduce a lot of volume and improve scanning performance by adding MEMS mirror. Although the maximum deflection angle of MEMS mirror is $\pm 12° \times \pm 6.5°$, when designing a wide-angle lens in Chapter 3.4, the maximum deflection angle cannot only consider the slow axis with a larger deflection angle. The deflection angle of the fast axis and the slow axis must be considered at the same time. That is, the

53

maximum deflection angle of the scanning mirror relative to the central axis istan$^{-1}(0.501457)° = 26.6317°$. If the superposition of the deflection angles of the slow axis and the fast axis is not considered, the scanned area will be its inscribed circle instead of the real scan range.
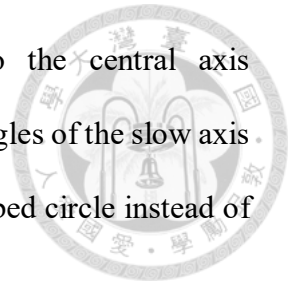
3.4   Wide angle scanning lens

Because the scanning angle of the MEMS mirror is only 24 degrees, we add a wide-angle scanning lens behind it. The traditional feasible method is to add an angle expansion optical system to the scanning system, which consists of two lenses-a positive lens behind the MEMS mirror and a negative lens behind it. However, this traditional lens set has at least two disadvantages[57]: (1) The divergence angle of the emitted light beam is too large. Although for short-distance targets, too large a laser divergence angle will not have a significant impact on scanning, but when used for targets tens of meters or hundreds of meters, the spot size of the outgoing beam will become larger. The energy per unit area is rapidly reduced, causing the returned laser signal to be too small. The SNR is too low to be received by the detector. (2) The expanded scanning angle is limited (usually less than 50 degrees). If the FOV increases, the distortion will become very serious. Therefore, we use the free-form surface technology to design the surface shape of the wide-angle lens into regions. With this technology, we not only designed a wide-angle lens that can expand the scanning range four times, but also controlled the maximum distortion value within 3%. This allows our wide-angle LiDAR system to achieve clear, large-angle scanning without distortion.

The wide-angle system we designed is composed of two parts: the lens near the

MEMS mirror is a positive lens, which slightly converges the parallel output light, and the other lens is a negative lens, which compensates for the converged beam and expands the beam exit angle. We use geometric optics light tracing simulation software Zemax, which includes design, optimization and analysis functions. In the Zemax original design editor, "entrance pupil" is set to the beam size reflected by the MEMS mirror, which is 0.5657 *mm*. However, this design has a disadvantage, because the beam diameter is small, it is not easy to observe the divergence of the beam, and it also makes the writing of the optimized function much more difficult. Therefore, the entrance pupil value will be increased during the design to make the designed lens more effective. The apodization type we chose is to be Gaussian, which imparts an amplitude variation over the pupil that is Gaussian in form . The "apodization factor" refers to the rate of decrease of the beam amplitude (or intensity) as a function of the radial pupil coordinate and is the same in both transverse directions. The beam amplitude is normalized to unity at the center of the pupil in ZEMAX, while at the other points in the entrance pupil is given by[59]

$$A(\rho) = e^{-G\rho^2} \tag{3.3}$$

where G and ρ are the apodization factor and the normalized pupil coordinate at the stop surface, respectively. Therefore, when G is equal to 1, the beam amplitude falls to the $1/e$ value (the intensity falls to $1/e^2$ value, about 13% of the peak) at the margin of the entrance pupil. In this design, we chose *G=1*.

Fig. 3.9　The simulated 3D layout of the wide-angle lens, each line of different color

represents the incident light at a different angle. The wide-angle lens system we

designed is a combination of a positive lens and a negative lens, and the detailed

structure of the lens surface is adjusted in different areas to improve the quality of the

laser beam in each scanning area. The maximum beam angle of the wide-angle lens

group is 104 degrees.

As shown in Fig. 3.9, our wide-angle lens is a combination of a positive lens and a

negative lens. The maximum beam angle of the wide-angle lens group is 104 degrees. It

can be obtained from the results of light tracing, because each beam of different angles is

evenly distributed on the image plane, so our design has almost no distortion. The

maximum deflection angle cannot only consider the slow axis with a larger deflection

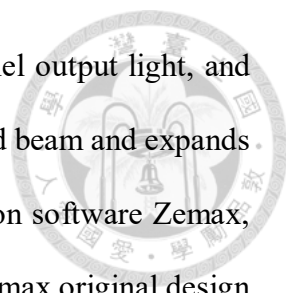angle, but must also consider the deflection angles of the fast axis and the slow axis. That

is, the maximum deflection angle of the scanning mirror relative to the central axis is

$\tan^{-1}(0.501457)° = 26.6317°$. If the superposition of the deflection angle of the slow axis

and the fast axis is not considered, the scanned area will be its inscribed circle instead of

the real scan range. In the Zemax simulation software, we input the maximum deflection

56

angle of the x-axis and the y-axis in the field angle field at the same time, instead of just inputting the maximum angle of a single direction. Because even if the optical system is axisymmetric, if one of the directions is ignored, it is easy to cause errors. Therefore, by entering the actual deflection angle value, although doing so will make the simulation process more difficult, it also makes the simulation result consistent with the real situation.

When designing the lens, we introduce the concept of free-form surface, cut the surface of the lens into many areas, and independently adjust the surface structure of each area. The lens surface is designed using an aspheric formula, as shown in the following equation.[59]

$$z = \frac{cr^2}{1 + \sqrt{1 - (1+k)c^2 r^2}} + \sum a_i r^{2i} \tag{3.4}$$

This formula is a binary function with many higher order terms. By adjusting the coefficient of the higher order term, the shape of the surface can be adjusted to our needs. With this design, we can get a wide-angle LiDAR that can scan long distances without distortion.

As shown in Fig. 3.11, the horizontal axis is the tilt angle of the MEMS mirror, and the vertical axis is the angle of the outgoing beam. It can be seen that the wide-angle lens set we designed can magnify the scanning angle of incident light uniformly by four times. Because the slope of this curve is almost a constant value, it means that each area of the lens can give almost the same magnification, so that the distortion value of the wide-angle lens group is very small.
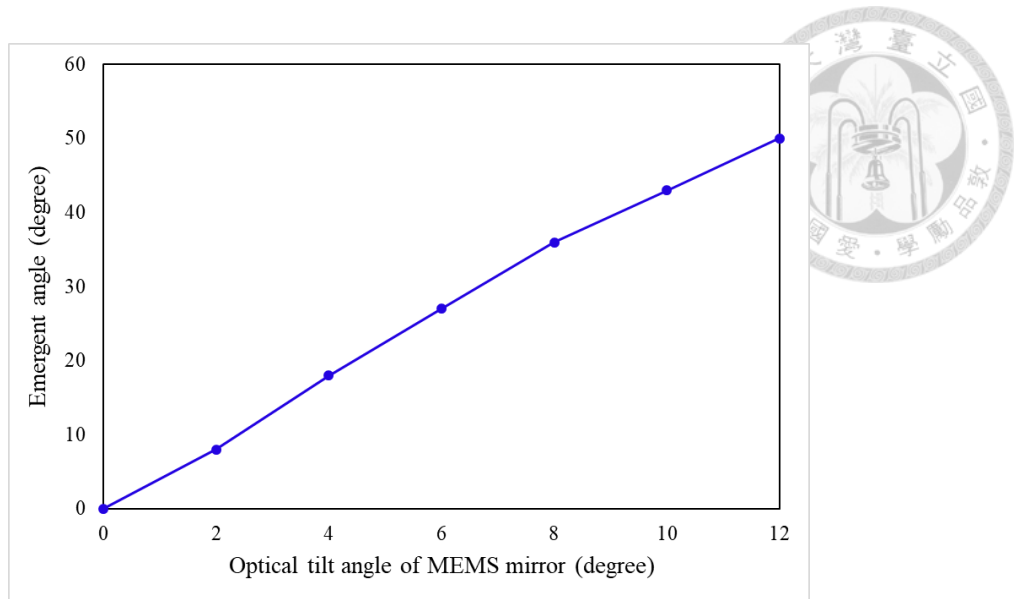
Fig. 3.10 The relationship between MEMS tilt angle and emergency angle.
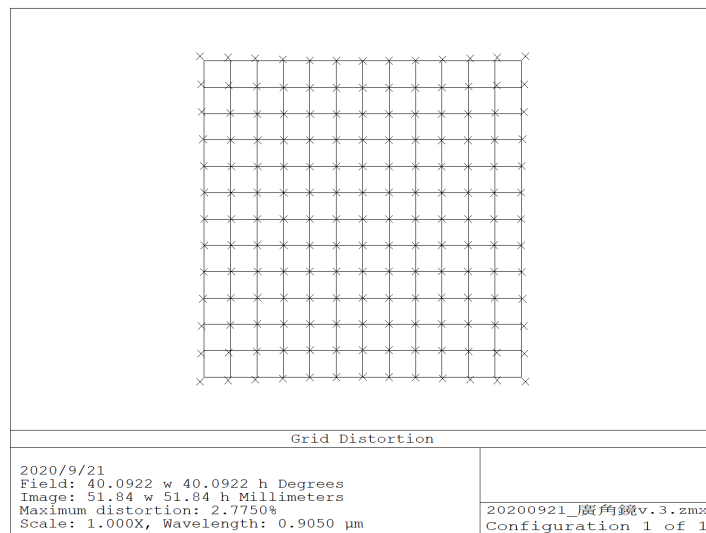
Fig. 3.11 The grid distortion of the Zemax wide-angle lens group simulation result. It must be noted that the value of Field represents the oblique angle, not the x-axis or y-axis. The maximum scanning angle of the wide-angle lens group we designed is 104 degrees.

After optimizing, the relative distortion of the wide-angle lens, which is given by[59]

$$D_T = \frac{tan\theta - \theta}{tan\theta} \times 100\%$$ (3.5)

is less than 3%.
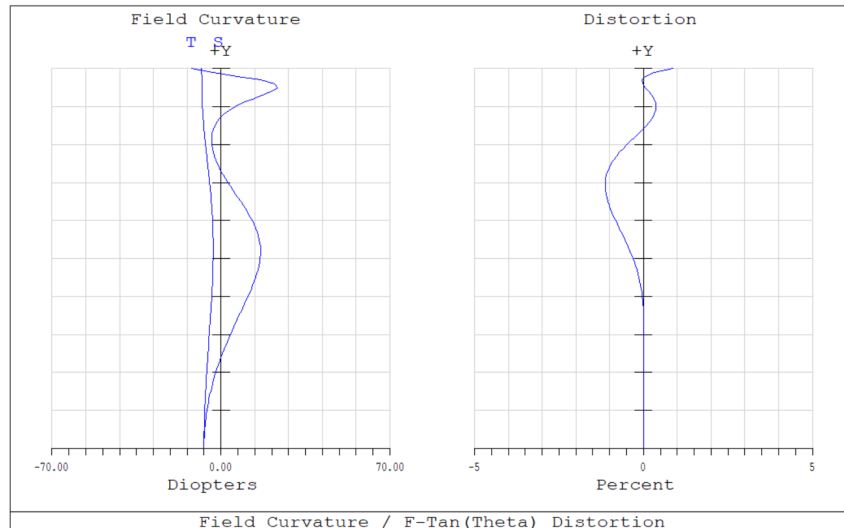
Fig. 3.12 Layout of wide-angle lens field curvature and distortion.

The spot sizes of different angles are shown in Fig. 3.13. The two lines from the upper left to lower right are the cases corresponding to the scan angle being (0°,0°), (0°,5°), (0°,10°), (0°,15°) ; (0°,20°), and (13°,24°), respectively. The spot size gradually increases with the increase of the angle, but they are all smaller than the airy disk, which meets the design requirements. We propose a 3D uniform scanning method based on MEMS, which achieves the design goal through only one positive lens and one negative lens. The maximum scanning angle of this wide-angle lens group is 104 degrees, and the distortion is less than 3%. Our design not only achieves a reduction in size and weight, but also reduces the number of optical components, which makes the entire LiDAR easier to assemble, and also increases the durability of the entire system. This greatly reduces the manufacturing cost of LiDAR and gives it more opportunities to be applied to many emerging applications.
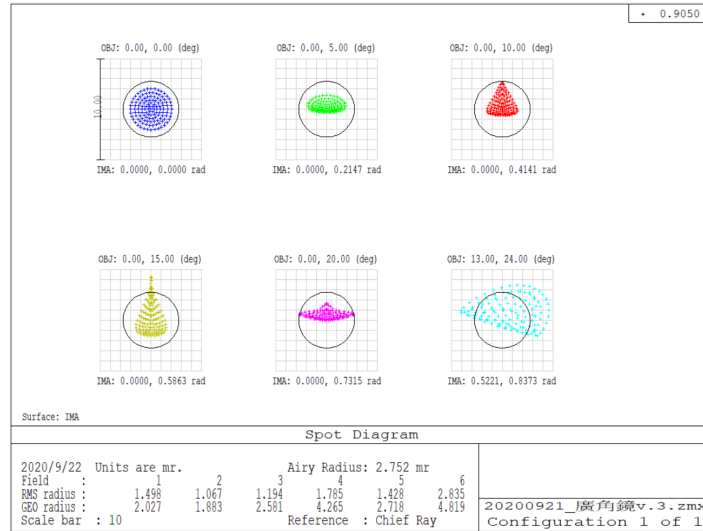
Fig. 3.13 Spot size with different scan angle in the target plane perpendicular to the optical axis at distance of about 100 m. The scale is 10 mrad, where the two lines from the upper left to lower right are the cases corresponding to the scan angle being (0°,0°), (0°,5°), (0°,10°), (0°,15°); (0°,20°), and (13°,24°), respectively.

3.5   Receiver lens design

The lens of the receiving system is designed to receive as much of the reflected laser beam signal as possible, and to converge the beam to the photodetector after the system for subsequent signal processing. The receiving lens of the LiDAR is independently designed, and different from the transmitting end wide-angle lens, it is composed of two aspheric lenses and adopts Avalance Photodiode (APD) (Thorlabs APD120A), as shown in Table 3.1. The receiving area of APD is 3*3mm. We choose Si-based APD because it can effectively detect optical signals with a wavelength of 905nm. APD is a detector that is extremely sensitive to optical signals, but in order to ensure that it can receive LiDAR optical signals at a large angle, we have designed a set of receiving lenses before APD. Due to the limitation of volume and weight, we design a system with a simple structure

60

as much as possible, and can not use a complex design. The receiving lens is modeled by Zemax to adapt to the wide-angle scanning of the transmitting. As shown in Fig. 3.14.
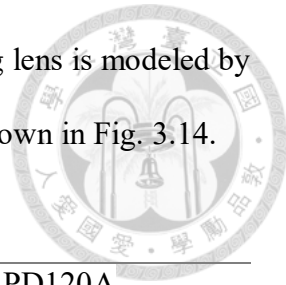
Type	Thorlabs APD120A
Detector Material	Silicon APD
Wavelength Range	400 to 1000 nm
Maximum APD Responsivity	25 A/W @ 800 nm, M=50
Active Area Diameter	3 mm
OUTPUT Bandwidth	DC to 50 MHz

Table 3.1 Si-APD detector parameters
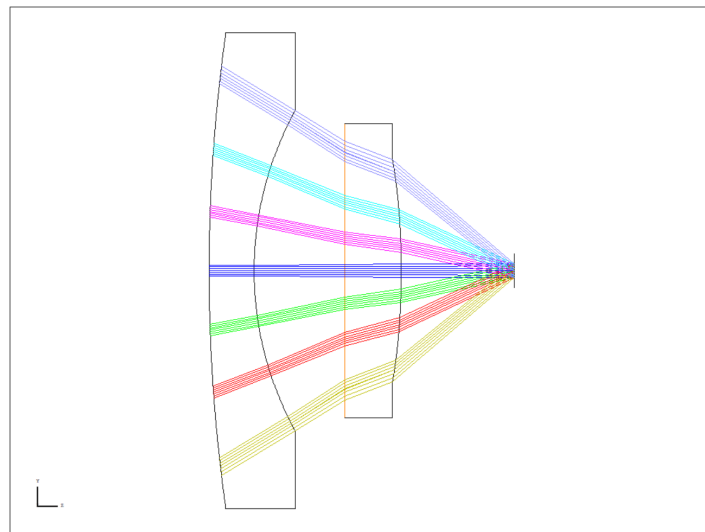
Fig. 3.14 Receiver lens Zemax layout.

As shown in Fig. 3.14, the receiving end lens is used to receive the light scattered by the target. The receiving end does not need a high resolution, because the ToF LiDAR imaging is to calculate the pulse signal of each point and combine it into a complete picture by MEMS, so the receiving end lens only needs to be designed to receive the

61
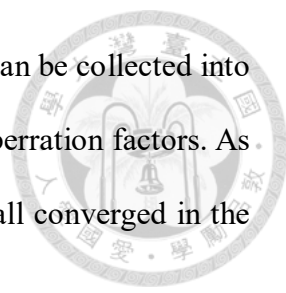
large-angle optical signal. That is, the light spots of different angles can be collected into the detection area of the detector, and there is no need to consider aberration factors. As shown in the figure below, the incident light at different angles are all converged in the detection area, so it meets the design requirements.
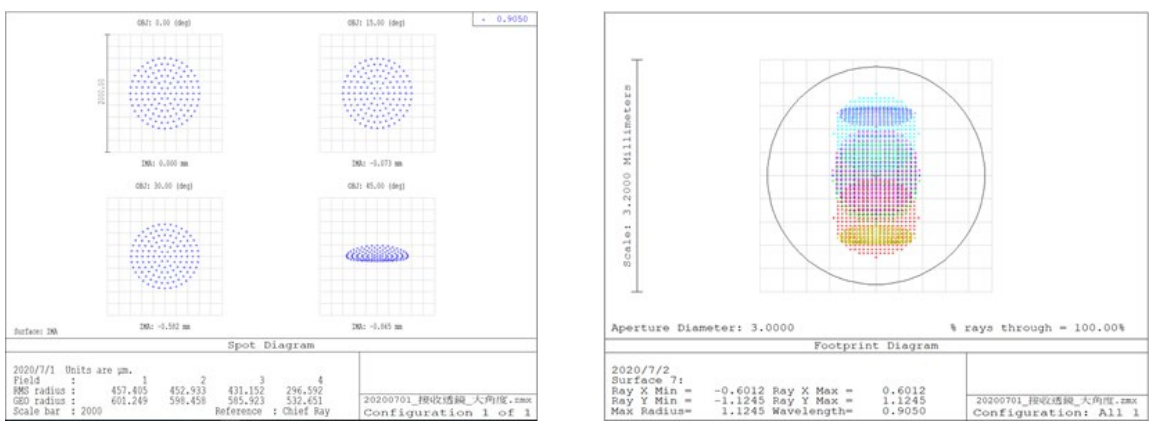
Fig. 3.15 Receiver lens Zemax spot diagram and footprint diagram layout. These two pictures respectively show the beam quality and distribution of the returned optical signal collected into the detection area.
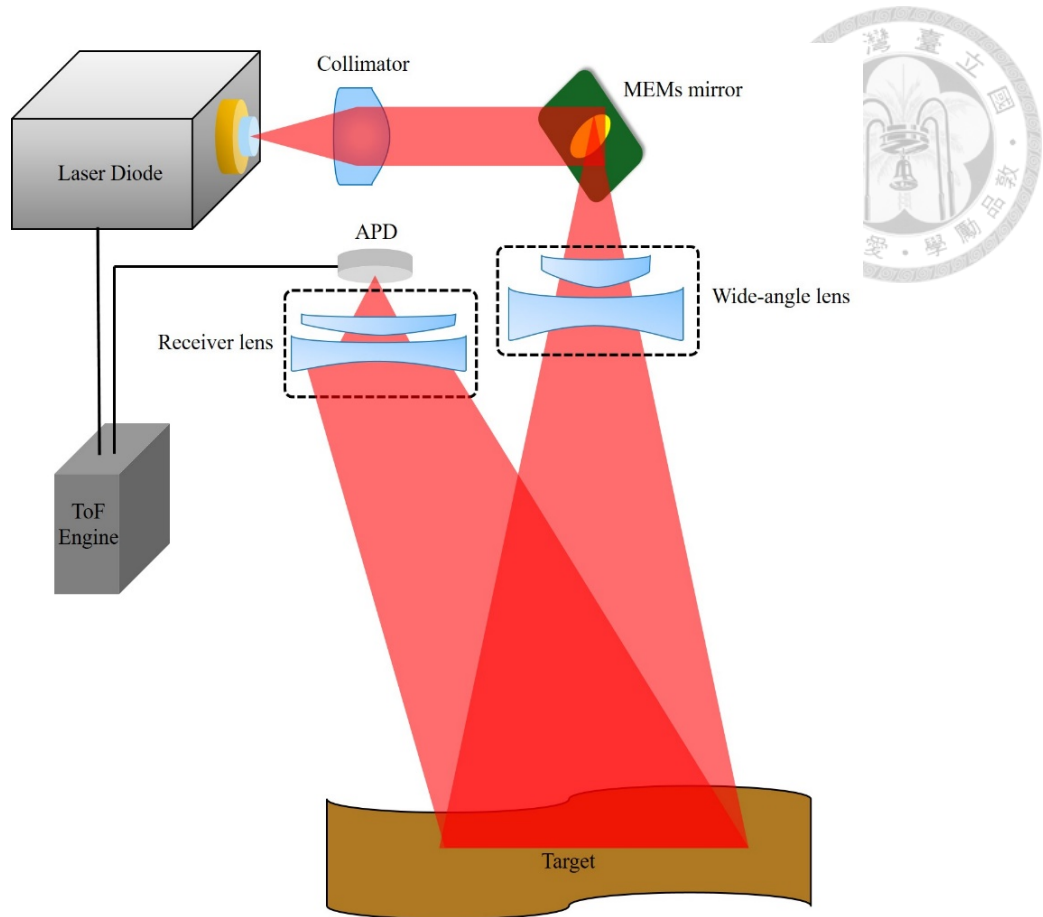
Fig. 3.16 Schematic diagram of wide-angle ToF LiDAR.

3.6　Compare wide-angle LiDAR with patents and papers

In order to compare the wide-angle LiDAR we designed with some patents, we looked for three patents that also use MEMS mirrors as scanning devices. Because in the application of autonomous driving, the scanning angle of LiDAR must reach more than 100 degrees. However, most of the current scanning technologies can scan very small angles, which means that it is more difficult to apply to automatic driving systems. The wide-angle LiDAR designed by us has a maximum scanning angle of more than 100 degrees, and with the self-designed wide-angle lens, the image quality is very good. The design method of Wide-angle lens is described in detail in Chapter 3.4. The patent 1 is "Wide field-of-view lidar optical assembly and system"[61], its scanning angle is 70 degrees, and the size of the system is not stated in the patent. It uses multiple laser beams and a rotatable wedge lens to divide each scanning direction, and uses a shutter to scan each angle with a different MEMS mirror. The patent 2 is "MEMS mirror with extended field of view useful for vehicle lidar"[62], its maximum scanning angle reaches 90 degrees, and a larger scanning range is combined through two or more MEMS mirrors. The patent 3 is "Device for optical imaging, tracking, and position measurement with a scanning MEMS mirror"[60], the patent owner is the famous MEMS mirror company Mirrorcle Technologies, Inc., they use a wide-angle lens in front of the MEMS mirror to expand the scanning angle, enlarge the original maximum tilt angle of 8 degrees to 45 degrees. In this patent, the setting of the receiver and the complete optical path structure are also fully explained. Table 3.2 compares the characteristics of the wide-angle lens we designed with three patents. Comparing these three patents with the system we designed, we can find that our system uses a MEMS mirror and a set of wide-angle mirrors composed of two lenses to achieve a wide-angle scanning of more than 100 degrees. And

also has a very good performance in imaging quality. Because of its simple structure, our LiDAR system has the characteristics of low cost and high performance.
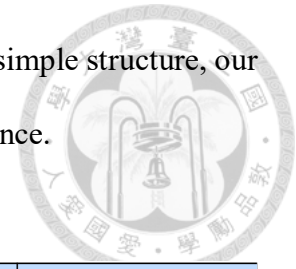
	Our design	Patent 1	Patent 2	Patent 3
Maximum scan angle	102°	70°	90°	45°
3D imaging principle	Time-of-flight (MEMS based laser scanning with wide-angle lens)	Time-of-flight (Multiple MEMS laser scanning with image stitching)	Time-of-flight (Multiple MEMS laser scanning with image stitching)	Time-of-flight (MEMS based laser scanning with wide-angle lens)
Size (mm)	150 × 50 × 25	-	-	-
Need image stitching	No	Yes	Yes	No

Table 3.2 Specifications of the system we designed, patent 1, patent 2 and patent 3.
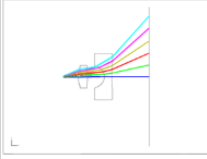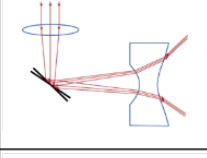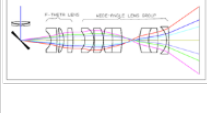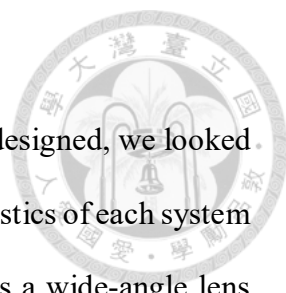
	Architecture	Maximum scanning angle	MEMS mirror scanning angle	Mirror dimension	Number of lenses
Our design		103°	±12°	1 mm	2
Paper 1		80°	±8°	4.3 mm	2
Paper 2		30°	±5°	5 mm	3
Paper 3		60°	±5.7°	3.6 mm	12

Table 3.3 Specifications of the system we designed, paper 1, paper 2 and paper 3.

In order to compare the performance of the wide-angle lens we designed, we looked for three scanning systems similar to ours and compared the characteristics of each system in Table 3.3. These three journal papers all use a MEMS mirror plus a wide-angle lens group to increase the scanning angle, but they all use different components and different numbers of lenses. The system we designed uses two aspherical lenses to allow the scanning angle to reach 103 degrees and control the distortion below 3%. The paper 1 is "Low-voltage wide-field-of-view lidar scanning system based on a MEMS mirror"[63], it also uses two aspheric lenses to expand the scanning angle, but the placement is slightly different from ours. The MEMS mirror it uses is 4.3 mm in diameter, and the maximum distortion is 4%. The paper 2 is "Design and realization of a wide field of view infrared scanning system with an integrated micro-electromechanical system mirror"[64]. It uses three lenses to achieve a 30-degree scanning angle, but because it has two surfaces plane, so it is more difficult to enlarge the scanning angle. The paper 3 is "Optical design of a new folding scanning system in MEMS-based lidar"[65], which uses a set of f-theta lens plus a wide-angle lens to expand the scanning angle to 60 degrees. Because it directly uses a whole set of f-theta lens, it has a very large number of lenses, which is larger and bulkier. The wide-angle lens we designed can magnify the scanning angle to 103 degrees, and through the carefully designed surface structure of the lens, the image quality is very good. In the comparison in Table 3.3, our wide-angle lens can reach the maximum scanning angle, and there is almost no distortion at the edge of the large-angle scanning image. There is a detailed introduction to our process of designing a wide-angle lens in Chapter 3.5.

Chapter 4　Experimental Setup and Data Processing

In order to demonstrate the scanning capabilities of our designed MEMS LiDAR and the effectiveness of the wide-angle lens, we modified the mechanical structure of the single-point laser rangefinder and added a MEMS mirror and wide-angle lens to successfully set up a LiDAR with a scanning angle of 100 degrees. . And through the point-cloud diagram image processing program we developed, the scanned data is converted into an image that can express depth information. Most of the LiDAR-related research in academia uses a laser diode with a power supply, plus a TCSPC computing system to get the depth information of each object, and finally the required optical components are installed on the optical platform. Although the advantage of doing so is that it is very convenient to modify the experimental architecture, and new components can be added to the system at any time. But if we experiment with this method, the final result is still very far from the actual commercialization, because the whole is very heavy and immovable, and the price is too expensive. Therefore, we abandon the use of benchtop instruments, and use OEM packaged distance measurement modules with EV kit modular MEMS mirrors. By doing this, there are no large-scale experimental instruments in the system we designed, and the power control and signal processing systems of all equipment are small IC circuit boards. And because of our experimental architecture design, the required power consumption is very low, the weight is also very light, and it can be moved around very conveniently, so the MEMS LiDAR system we designed is very close to the actual market demand. In Chapter 4.1, the role of each component will be introduced in detail. In Chapter 4.2, the principles of the experimental architecture will be introduced in detail. Finally, in Chapter 4.3, we will explain the operation method of the image processing program we wrote.
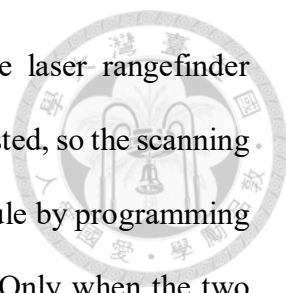
4.1   Material used for the experiment

The wide-angle LiDAR system we demonstrated is modified from Garmin LiDAR lite v.3. Both the laser transmitter module and the optical signal receiver module are modified from the laser rangefinder, but because the size of the laser beam is different from the MEMS mirror, we added a set of telescope structures (Thorlabs LA1251-B, LC2969- B), so that the laser light can be completely irradiated on the mirror. Regarding the scanning system, we use a MEMS mirror (UM-6002G) produced by UltiMEMS. This MEMS mirror is a package in the form of an EV-kit, and its movement is controlled by a drive circuit board. The laser rangefinder uses the Arduino Uno as the control circuit. By writing the Arduino language, the pulse frequency of the laser and the receiving frequency of the light signal are controlled, and the depth information of each point in the space is received on the Arduino control system. Table 4.1 shows the parameters and functions of each part in the LiDAR system.

Item	Function
Laser range-finder	Garmin LiDAR lite v.3 operates at 5V DC with a current consumption rate of <100mA at continuous operation. On top of everything else, it can be interfaced via I2C or PWM with the included 200mm accessory cable. It has a distance measurement capability of 40 meters when measuring objects with 70% reflectivity. The minimum measurement speed is 50 points per second. In I2C high-speed mode, 1000 points can be measured per second.
MEMS mirror	UltiMEMS UM-6002G EV-kits. Package dimension: 9.6*4.7*2.0 (mm) Mirror size: 1.0*1.4 (mm) Scan angle(mechanical): $\pm12°$(fast) $\times \pm6.5°$(slow) Frequency: 27000 (fast) DC to 500 (slow)
Micro-controller	Arduino Uno Rev3. It has 14 digital input/output pins (of which 6 can be used as PWM outputs), 6 analog inputs, a 16 MHz ceramic resonator (CSTCE16M0V53-R0), a USB connection, a power jack, an ICSP header and a reset button. It can connect to a computer with a USB cable or power it with a AC-to-DC adapter or battery to get started.
Beam expender	Thorlabs LA1251-B，LC2969-B. Because the beam size of the laser module is 1.2 mm, which is larger than the area of the MEMS mirror, in order to effectively let all the laser light reflect through the mirror, a set of optical systems that can reduce the beam size are designed using the principle of a telescope.
Structure	The self-designed movable support frame is manufactured by using a 3D printer (Stratasys Object 24) with extremely high precision (0.028 mm printing thickness). Through 3D printing technology, optical components can be assembled quickly and accurately, and a movable LiDAR system can be produced.
Software interface	Write the control system of the laser rangefinder on the arduino control interface, and after adjusting the detection rate, pulse speed and other parameters of the rangefinder, you can start scanning together with the MEMS mirror. Our communication uses I2C mode. The signal obtained after scanning is displayed in a digital type, and the digital numbers are integrated into a point cloud through a self-developed image processing program.

Table 4.1 Material used for the experiment.

Because our wide-angle LiDAR system is modified from the laser rangefinder module, the emission intensity of the laser light source cannot be adjusted, so the scanning range is fixed. We adjust the operating mode of the rangefinder module by programming the Arduino, and match it with the vibration of the MEMS mirror. Only when the two work together can we get a complete scan result. After the scan is completed, the result obtained is presented in digital form, that is, the depth information of each point in space and its coordinate position. It needs to be imported into an image processing program to be able to be converted into a clearer and easier to interpret 3D point cloud map. In chapter 4.2, we will discuss the details of system setup. In Chapter 4.3, the method of generating 3D point cloud images will be discussed in detail.

4.2   Experimental setup

All the instruments in our wide-angle LiDAR system use the plastic support structure and shell designed and made by ourselves to complete the system erection. Although this method of setting up the instrument is the most suitable design for the actual application, it will not be possible to modify the structure once the plastic model is completed, so pre-optical simulation will become very important. Our system has undergone a complete optical system simulation before implementation, including ray tracing analysis, light field intensity analysis in each area, scattering analysis and atmospheric influence factor analysis. In Zemax optical simulation software, a non-sequential mode with external environmental interference factors is used to construct a scanning system. The plastic support structure is drawn by Solidworks, which is a multi-functional drawing software for drawing three-dimensional graphics, and it can work with the optical simulation

software Zemax, that is, 3D objects designed by yourself can be imported into Zemax for optical simulation. As shown in Fig. 4.1, this is the result of drawing the plastic support structure of the LiDAR system in Solidworks. The laser rangefinder is directly placed on the support frame, followed by a lens group to adjust the beam size, and finally it scans the space after being reflected by the MEMS mirror. In Fig. 4.1, the wide-angle lens has not been added for experiments, so the scanning angle is small, so there is no need to modify the structure of the laser rangefinder to receive the reflected beam signal. In this experiment, we directly match the laser rangefinder with the MEMS mirror to get a small-scan LiDAR system. However, in order to test the performance of the wide-angle lens we designed, we will finally discuss how to modify the system to complete a large-angle scan in the following chapters.
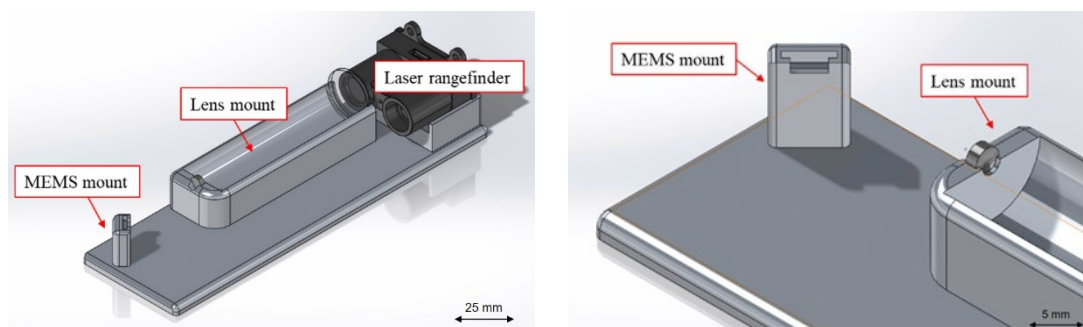
Fig. 4.1   The plastic support structure of the LiDAR system is drawn in the computer aid graphic software Solidworks.
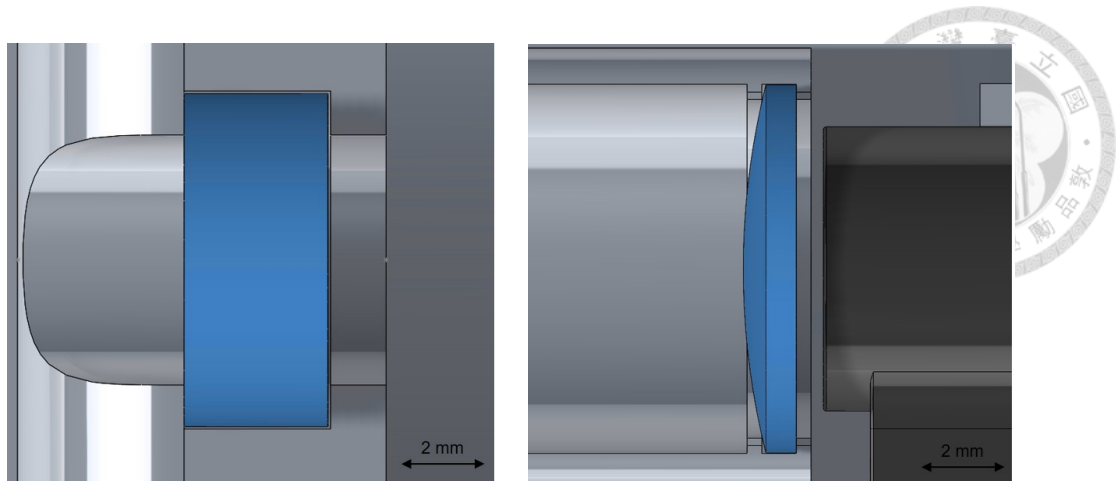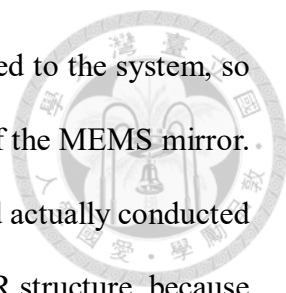
Fig. 4.2　The 3D printed lens support structure is designed with a tolerance of 0.04 mm, so that the lens can be inserted smoothly when the lens is installed. The blue part in the picture is the lens.

Although today's 3D printers can print highly accurate plastic structures, the impact of tolerances on the system combination must still be considered. When we originally designed the support frame, we directly used the size of the lens to design a set of support frame and printed it out, but because it was too close to the size of the lens, the lens could not be installed into the system smoothly. After this failed experience, we compared the equipment specifications of commercially available lens and optical experiment equipment manufacturers and found that if a tolerance of 0.04mm is added to the design of the lens and the support frame, the assembly of the lens can be successfully carried out. As shown in Fig. 4.2. Therefore, the final experimental framework took into account the design of tolerances, and successfully designed a support frame that can be inserted into the lens. But because the wavelength of the laser light source we use is 905 nm, which belongs to the infrared light band and cannot be seen directly by human eyes, the laser must be used to observe the card repeatedly when setting up the system to ensure that the laser beam is completely injected into the MEMS mirror.

72

In this LiDAR architecture, a wide-angle lens has not been added to the system, so the scanning angle is only 24 degrees of the mechanical deflection of the MEMS mirror. We then designed a support structure that can add a corner mirror, and actually conducted experiments to test the wide-angle scanning capability. In this LiDAR structure, because the processing time of the wide-angle lens is long, the wide-angle lens in the system is borrowed from Ultimems to test the scanning capability of the wide-angle LiDAR. Fig. 4.3 is a MEMS mirror mounted on a plastic support frame. Behind the MEMS mirror is its control circuit board and Arduino microcontroller. The laser beam is first adjusted by the beam expender, reflected by the MEMS mirror, and then passed through the wide-angle lens to increase the scanning angle.

However, after experiments, it was found that because the laser light transmitting and receiving modules in the LiDAR system were modified using a modular laser rangefinder, in addition to the beam size of the transmitting end, the structure of the receiving end must also be modified. , So that the large-angle light signal can enter the photodetector. Related research in the past found that if the lens and housing in front of the receiving end are removed, a wide-angle optical signal can be received[25]. As shown in Fig. 4.4, although the receiver lens can increase the detection range of LiDAR, that is, it can increase the receiving ability of weak reflected light signals, but it severely limits the optical signal receiving angle of the system. If the receiver lens is removed, the limitation on the receiving angle of the optical signal can be lifted. But doing so will limit the detection range of the LiDAR system, because after the receiver lens is released, the weak light signal returned from the original distance will not be received, and the scanning distance of our LiDAR system is limited to 200 cm. After experiments, our wide-angle LiDAR system can scan at an angle of 100 degrees, and finally generate a 3D point cloud image through a self-designed image processing program. The calculation

73

process of the point cloud will be discussed in Chapter 4.3.
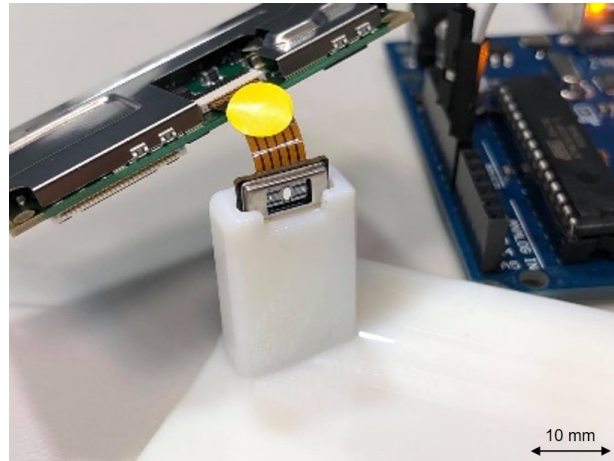
Fig. 4.3　MEMS mirror mounted on a plastic support frame. The laser beam is first adjusted by the beam expender, reflected by the MEMS mirror, and then passed through the wide-angle lens to increase the scanning angle.
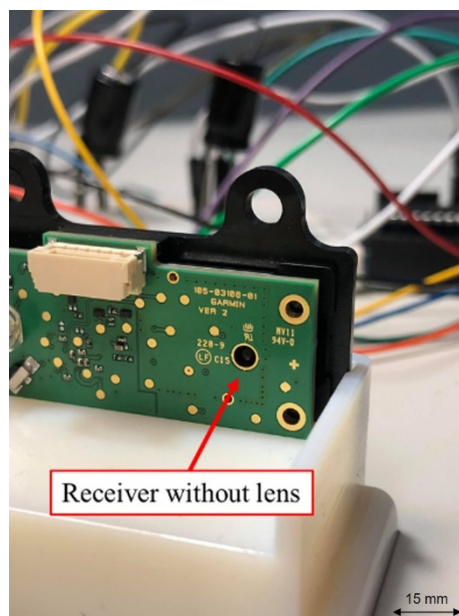
Fig. 4.4　Removed the receiver of the lens. Although the receiver lens can increase the detection range of LiDAR, that is, it can increase the ability to receive weak reflected

74

light signals, but it severely limits the optical signal receiving angle of the system. If the receiver lens is removed, the limitation on the receiving angle of the optical signal can be lifted.

Fig. 4.5   Wide-angle LiDAR system installed in a protective case.

As shown in Fig. 4.5, in order to better demonstrate the lightweight and small size characteristics of the wide-angle LiDAR, we designed its protective case to house all the messy wires and control circuit boards and other parts. By doing this, if you need to move the LiDAR system for other measurements, you don't need to disassemble the originally set up system and then reassemble it on the optical table. You only need to remove the power cord of the USB interface. Pick up the entire system. In this paper, by introducing a MEMS mirror as a laser scanner, the weight of LiDAR is greatly reduced. A wide-angle lens is added in front of the MEMS mirror, which magnifies the original mechanical deflection of the MEMS mirror by four times to achieve a large-angle scan of 100 degrees. In Table 4.2, the field-of-view required for different LiDAR applications are compared. The LiDAR we designed has a scanning angle of 100 degrees, reaching the level of

75

application in automated driving systems. Most of the current LiDAR systems on the market use mechanical motors to drive the entire scanning lens, which makes the entire system very heavy. In Table 4.4, we have consolidated the weight of each part of the wide-angle LiDAR system we designed. Our system weighs only 230 grams, which is very light compared to the other commercially available LiDARs in Table 4.6 and can be widely used in many applications.
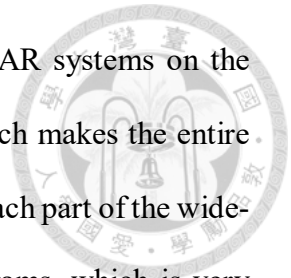
Applications	FOV($^\circ$)	Mirror Size (mm)	Resonant Frequency (kHz)
Self-Driving Cars (Adaptive Cruise Control)	25	2	0.8
Self-Driving Cars (Cross Traffic Alert)	80	1	0.5
Blind-Spot Detection	120	1	0.5
Gesture Recognition	50	0.5	0.2
Ground Robotics	25	1	0.2
Micro Air Vehicles (MAVs)	30	1	0.4

Table 4.2 Compare the FOV required by various LiDARs with other important parameters.

Item	Weight	Specification
Laser rangefinder	22 g	Garmin lidar lite v.3
Beam expander lens group	29 g	Thorlabs stock lens
MEMs system	33 g	Ultimems Inc.
Micro-controller	25 g	Arduino Uno
System shell	121 g	Print by 3D printer
Whole system	230 g	$150 \times 50 \times 25$ (mm)

Table 4.3 The weight of each part of the wide-angle LiDAR we designed and the size of the entire system.

Item	Weight
Velodyne HDL-32E	690 g
YellowScan VX-20	3100 g
Routescene UAV LidarPod	2800 g

Table 4.4 The weight of a commercially available LiDAR system.

4.3　Generate point-cloud diagram

The wide-angle LiDAR we designed is based on the ToF principle and uses the flight time of the beam to calculate the distance between the object and the light source. In addition to adding a MEMS mirror and a wide-angle lens, in addition to extending the one-dimensional single-point laser range measurement into a three-dimensional space detection, it also increases the field-of-view of the system through the wide-angle lens to achieve a small size and high-performance LiDAR scan system. Through the scanning of our wide-angle LiDAR system, the depth relationship of each position in space can be captured on the computer. But if only the distance between the position of each object in the space and it can be obtained, only a large number of digits will be displayed. Therefore, we developed an image processing program by ourselves, which was written in python. The scan result of the LiDAR system is to use the display window in the Arduino control program to read the spatial information, and export it into a file in the form of txt. Then these files with only digital information are imported into the image processing program and combined into one a picture showing depth information using color. Because the ranging unit in our scanning system, namely the laser light source and photodetector, uses a modular laser rangefinder, the hardware architecture cannot be changed too much, so we independently design the ranging unit and the imaging unit. Because the equipment manufacturer of the laser rangefinder only provides the option of using Arduino control, we developed the image processing unit with python separately, and imported the data measured by LiDAR into it to form a point cloud image. Our system limits the number of points detected due to the limitation of the performance of the ranging module. In Fig. 4.7, there are 1000 distance data points in the vertical direction, and one data point every

78

degree in the horizontal direction. As shown in Fig. 4.6, we place cardboards at different distances in the corridor, and use our LiDAR to scan its depth relationship, and in Fig. 4.7, the detected data is processed into a depth image showing the distance in different colors.
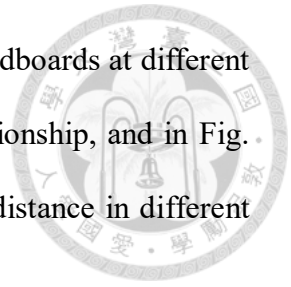
Fig. 4.6　Place cardboards at different distances on the floor, and use our LiDAR to scan its depth relationship.
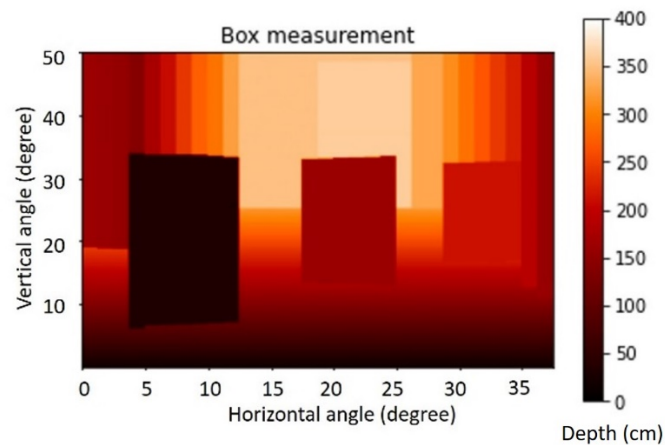

Fig. 4.7　The depth image calculated using the detected data.

In Fig. 4.7, the scanning system has not added a wide-angle lens, so the range that can be scanned is small. We then tested the effect of the wide-angle lens installed in the scanner. As mentioned in section 4.2, because the lens at the receiving end of the ranging

module severely limits the maximum measurement angle, the lens and lens housing in front of it are removed to increase the angle of the maximum receiving optical signal. But doing so will affect the farthest distance that can be detected, because after removing the lens at the receiving end, the photodetector cannot detect the weak light signal bounced back from the distant target. When we measure LiDAR with a wide-angle lens, we place the target closer to ensure that we can receive the optical signal at every angle. In Fig. 4.8, we use LiDAR with a wide-angle lens and LiDAR without a wide-angle lens to scan the target object. According to the results of the scan, the field-of-view of the LiDAR with the wide-angle lens has been increased to 100 degrees, which allows the scanning range to be larger. Finally, we adjusted the fast axis of the MEMS mirror to be parallel to the ground, so that the horizontal field-of-view of the scanning range reached 100 degrees. As shown in Fig. 4.11, we made the abbreviation "NTU" of National Taiwan University and scanned it with a wide-angle LiDAR to compare the difference before and after adding a wide-angle lens.

Fig. 4.8 The scanned object. The results of the scan are shown in Fig. 4.9 and Fig. 4.10.
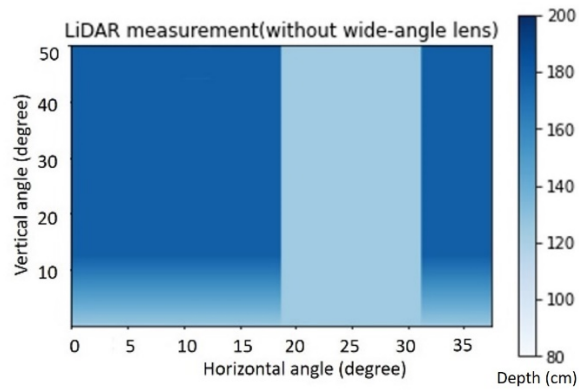
Fig. 4.9   The scan result of the wide-angle lens has not been added.

Fig. 4.10 After adding the wide-angle lens, the maximum scanning angle reaches 100

degrees.

Fig. 4.11 We made a "NTU" card and scanned it with LiDAR to compare the difference

before and after the wide-angle lens was added. The results of the scan are shown in
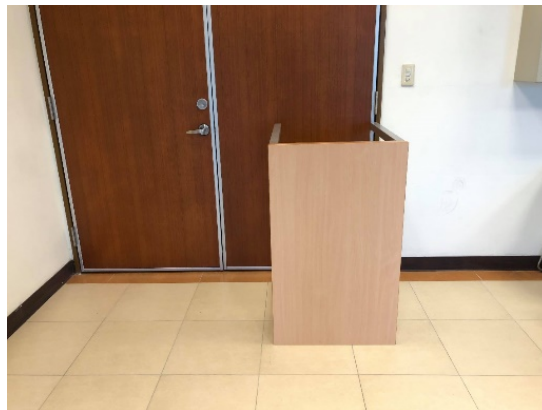
Fig. 4.12 and Fig. 4.13.
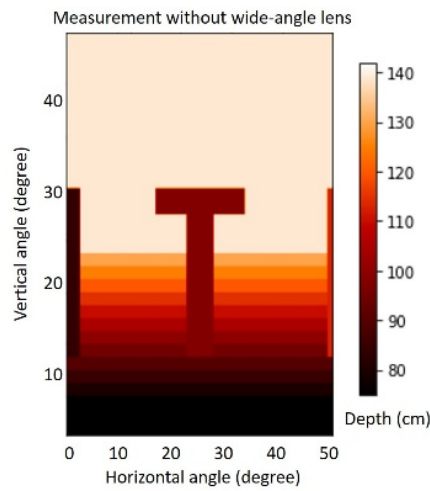
Fig. 4.12 The scan result of the wide-angle lens has not been added.

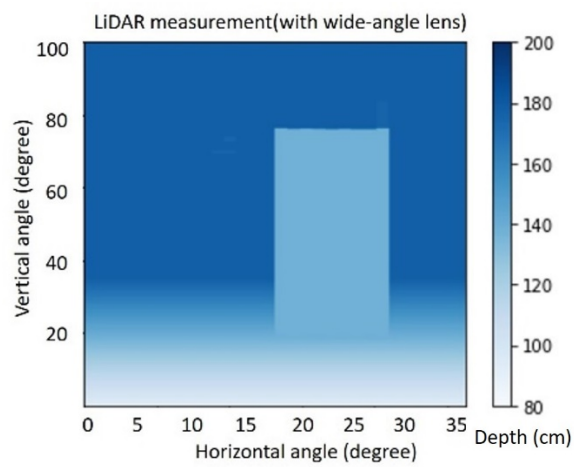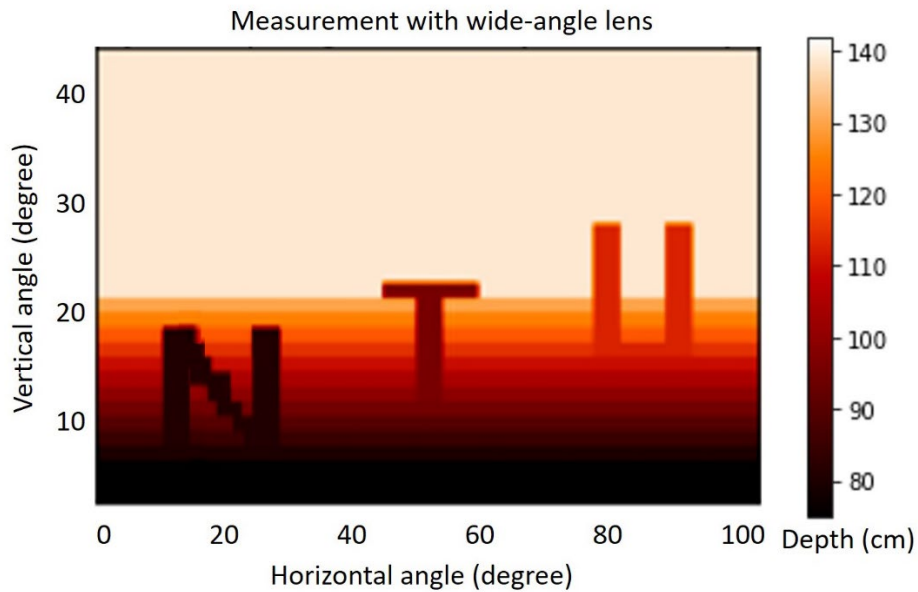Fig. 4.13 Add the scan result of the wide-angle lens. In this scan, we rotated the

scanning direction of the entire system by 90 degrees, so that the maximum horizontal

angle reached 100 degrees.

We summarize the error of the scanning result of each angle as shown in Fig. 4.14, and the target when measuring the error is set at 2.5 meters away. Because the wide-angle lens is axisymmetric, we measured the scan error from 0 degrees to 50 degrees. Here we define scanning error $\Delta h \equiv h' - h$, where h' is the actual measurement result value, and h is the actual distance. After the calculation, the Δh generated is divided by the actual distance of the target to obtain the scanning error expressed as a percentage. From the measurement results, the measurement error of our LiDAR system is very small, so we can get very good quality images.
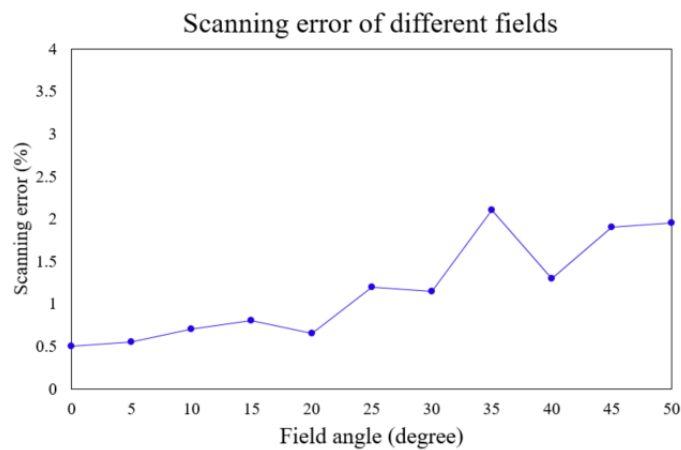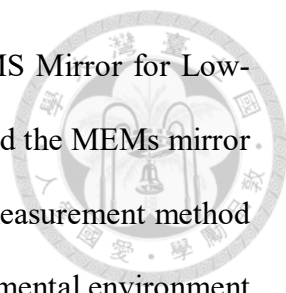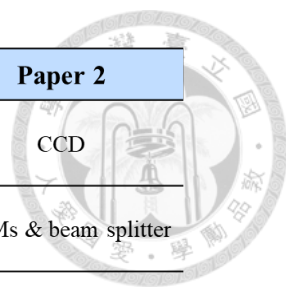
Fig. 4.14 The measurement error of each angle, the target is set at 2.5 meters away. At large angles, because the beam diameter is large and the incident angle of the light beam received by the photodetector is large, the intensity of the light signal per unit area is low, so the error is relatively large. However, the maximum error value is within 2.5%, which has almost no effect on the imaging quality of the point cloud diagram.

4.4   Compare system structure with papers

We compare the system architecture we designed with the two latest journal papers this year, and list many of the parameters used to test the performance of LiDAR in Table

4.5. Paper 1 is "A Low-Voltage, Low-Current, Digital-Driven MEMS Mirror for Low-Power LiDAR"[22]. This journal paper uses a laser rangefinder to add the MEMs mirror deflected scanning beam, so their system architecture and distance measurement method is similar to ours. However, their imaging quality is poor. The experimental environment is carried out without external light interference. The target object is scanned with a material with high reflectivity, and the final point cloud image obtained also has a high error value. Paper 2 is "Simultaneous Enhancement of Scanning Area and Imaging Speed for a MEMS Mirror Based High Resolution LiDAR"[35]. Although the light source and scanning structure of this journal paper are similar to ours, they do not use 3D ranging methods, but directly use CCD to shoot images. From the comparison in Table 4.5, we can see that our LiDAR system has the best scanning quality, the scanning angle is also the largest, and it can be measured in normal ambient light. The system we designed is small in size, light in weight, low in power consumption and excellent in imaging quality, making it a good choice for further development.

	This work	**Paper 1**	**Paper 2**
Imaging Principle	ToF	ToF	CCD
Optical system	MEMs & wide-angle lens	MEMs	MEMs & beam splitter
Channel	1	1	2
Maximum scanning angle	100°	-	52°
Laser Wavelength (nm)	905	905	635
Laser power (W)	1.3	10	0.01
Target reflectivity	30%	80%	30%
Background light (lux)	500	0.0003	0.0003
Error	2%	17%	-

Table 4.5 Comparison of performance parameters between our LiDAR and journal papers with similar system architectures.

Chapter 5 　 Conclusion

In this thesis, we propose an optical system design and performance optimization method for a LiDAR scanning system based on MEMS mirror and wide-angle lens, and fabricate a small and lightweight MEMS LiDAR. The weight of the entire system is less than 230 g. The volume is 150 mm×50 mm×25 mm, and through the ToF calculation method, the image processing program is developed to generate the point cloud image. Through the system we designed, we demonstrated a wide-angle LiDAR with a FoV of 100 degrees. We use Zemax to design all the optical lenses in the system, including collimator, laser scanning system, wide-angle lens and receiver lens. In order to expand the scanning angle, we proposed a method of designing a high-performance wide-angle lens, and designed a wide-angle scanning lens that can magnify the scanning angle of the MEMS mirror to 100 degrees and the distortion is less than 3 %. It is worth mentioning that the use of MEMS mirror on the scanning device can achieve a smaller size and faster scanning speed, with high efficiency, large field of view, simple structure, low power consumption and light weight, which means that the 3D image LiDAR has very application value. In the 2 klux natural light environment, the wide-angle LiDAR is measured and analyzed. The maximum error is 4.1 cm, so the error is within 2 %. Finally, a self-written image processing program was used to convert the scanned data into a 3D point cloud image, and the generated image proved the complete function of LiDAR.
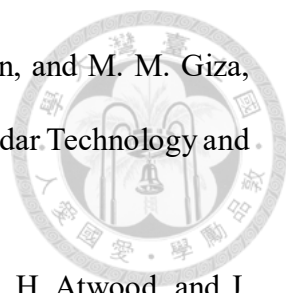
REFERENCE
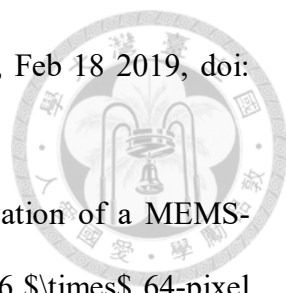
[1] D. Wang, C. Watkins, and H. Xie, "MEMS Mirrors for LiDAR: A review," *Micromachines (Basel),* vol. 11, no. 5, Apr 27 2020, doi: 10.3390/mi11050456.

[2] S. Royo and M. Ballesta-Garcia, "An Overview of Lidar Imaging Systems for Autonomous Vehicles," *Applied Sciences,* vol. 9, no. 19, 2019, doi: 10.3390/app9194093.

[3] T. Raj, F. H. Hashim, A. B. Huddin, M. F. Ibrahim, and A. Hussain, "A Survey on LiDAR Scanning Mechanisms," *Electronics,* vol. 9, no. 5, 2020, doi: 10.3390/electronics9050741.

[4] S.-H. Chung, S.-W. Lee, S.-K. Lee, and J.-H. Park, "LIDAR system with electromagnetic two-axis scanning micromirror based on indirect time-of-flight method," *Micro and Nano Systems Letters,* vol. 7, no. 1, 2019, doi: 10.1186/s40486-019-0082-9.

[5] G. Kim and Y. Park, "LIDAR pulse coding for high resolution range imaging at improved refresh rate," *Opt Express,* vol. 24, no. 21, pp. 23810-23828, Oct 17 2016, doi: 10.1364/OE.24.023810.

[6] F. Schwarz *et al.*, "Resonant 1D MEMS mirror with a total optical scan angle of 180° for automotive LiDAR," presented at the MOEMS and Miniaturized Systems XIX, 2020.

[7] N. Radwell, A. Selyem, L. Mertens, M. P. Edgar, and M. J. Padgett, "Hybrid 3D ranging and velocity tracking system combining multi-view cameras and simple LiDAR," *Sci Rep,* vol. 9, no. 1, p. 5241, Mar 27 2019, doi: 10.1038/s41598-019-41598-z.

[8]   L. A. Eldada, E.-H. Lee, S. He, G. Kim, J. Eom, and Y. Park, "Design and implementation of 3D LIDAR based on pixel-by-pixel scanning and DS-OCDMA," presented at the Smart Photonic and Optoelectronic Integrated Circuits XIX, 2017.

[9]   K. Kuzmenko *et al.*, "3D LIDAR imaging using Ge-on-Si single-photon avalanche diode detectors," *Opt Express,* vol. 28, no. 2, pp. 1330-1344, Jan 20 2020, doi: 10.1364/OE.383243.

[10]   R. Tobin, A. Halimi, A. McCarthy, M. Laurenzis, F. Christnacher, and G. S. Buller, "Three-dimensional single-photon imaging through obscurants," *Opt Express,* vol. 27, no. 4, pp. 4590-4611, Feb 18 2019, doi: 10.1364/OE.27.004590.

[11]   Y. Takashima *et al.*, "Development of coaxial 3D-LiDAR systems using MEMS scanners for automotive applications," presented at the Optical Data Storage 2018: Industrial Optical Devices and Systems, 2018.

[12]   J. Tachella *et al.*, "Real-time 3D reconstruction from single-photon lidar data using plug-and-play point cloud denoisers," *Nat Commun,* vol. 10, no. 1, p. 4984, Nov 1 2019, doi: 10.1038/s41467-019-12943-7.

[13]   X. Zhou, G. Li, J. Huddleston, and A. A. Chesworth, "Precision optical components for lidar systems developed for autonomous vehicles," presented at the Next-Generation Optical Communication: Components, Sub-Systems, and Systems VII, 2018.

[14]   C. I. Rablau, A.-S. Poulin-Girard, and J. A. Shaw, "Lidar: a new self-driving vehicle for introducing optics to broader engineering and non-engineering audiences," presented at the Fifteenth Conference on Education and Training in Optics and Photonics: ETOP 2019, 2019.

[15]   G. Kim and Y. Park, "Independent Biaxial Scanning Light Detection and Ranging

System Based on Coded Laser Pulses without Idle Listening Time," *Sensors (Basel),* vol. 18, no. 9, Sep 4 2018, doi: 10.3390/s18092943.

[16]   A. McCarthy *et al.*, "Kilometer-range, high resolution depth imaging via 1560 nm wavelength single-photon detection," *Opt Express,* vol. 21, no. 7, pp. 8904-15, Apr 8 2013, doi: 10.1364/OE.21.008904.

[17]   B. Smith, B. Hellman, A. Gin, A. Espinoza, and Y. Takashima, "Single chip lidar with discrete beam steering by digital micromirror device," *Opt Express,* vol. 25, no. 13, pp. 14732-14745, Jun 26 2017, doi: 10.1364/OE.25.014732.

[18]   M. J. Sun *et al.*, "Single-pixel three-dimensional imaging with time-based depth resolution," *Nat Commun,* vol. 7, p. 12010, Jul 5 2016, doi: 10.1038/ncomms12010.

[19]   M. J. Sun and J. M. Zhang, "Single-Pixel Imaging and Its Application in Three-Dimensional Reconstruction: A Brief Review," *Sensors (Basel),* vol. 19, no. 3, Feb 11 2019, doi: 10.3390/s19030732.

[20]   G. Zhou, Z. H. Lim, Y. Qi, and G. Zhou, "Single-Pixel MEMS Imaging Systems," *Micromachines (Basel),* vol. 11, no. 2, Feb 20 2020, doi: 10.3390/mi11020219.

[21]   K. Dholakia *et al.*, "Real-time 3D video utilizing a compressed sensing time-of-flight single-pixel camera," presented at the Optical Trapping and Optical Micromanipulation XIII, 2016.

[22]   D. Wang, L. Thomas, S. Koppal, Y. Ding, and H. Xie, "A Low-Voltage, Low-Current, Digital-Driven MEMS Mirror for Low-Power LiDAR," *IEEE Sensors Letters,* vol. 4, no. 8, pp. 1-4, 2020, doi: 10.1109/lsens.2020.3006813.

[23]   R. Moss *et al.*, "Low-cost compact MEMS scanning ladar system for robotic applications," presented at the Laser Radar Technology and Applications XVII, 2012.

[24] M. D. Turner, G. W. Kamerman, B. L. Stann, J. F. Dammann, and M. M. Giza, "Progress on MEMS-scanned ladar," presented at the Laser Radar Technology and Applications XXI, 2016.

[25] M. D. Turner, G. W. Kamerman, A. Kasturi, V. Milanovic, B. H. Atwood, and J. Yang, "UAV-borne lidar with MEMS mirror-based scanning capability," presented at the Laser Radar Technology and Applications XXI, 2016.

[26] G. W. Kamerman *et al.*, "A compact 3D lidar based on an electrothermal two-axis MEMS scanner for small UAV," presented at the Laser Radar Technology and Applications XXIII, 2018.

[27] C. Zhu, M. J. Hobbs, M. P. Grainger, and J. R. Willmott, "Design and realization of a wide field of view infrared scanning system with an integrated micro-electromechanical system mirror," *Appl Opt,* vol. 57, no. 36, pp. 10449-10457, Dec 20 2018, doi: 10.1364/AO.57.010449.

[28] X. Lee, C. Wang, Z. Luo, and S. Li, "Optical design of a new folding scanning system in MEMS-based lidar," *Optics & Laser Technology,* vol. 125, 2020, doi: 10.1016/j.optlastec.2019.106013.

[29] A. McCarthy *et al.*, "Kilometer-range depth imaging at 1,550 nm wavelength using an InGaAs/InP single-photon avalanche diode detector," *Opt Express,* vol. 21, no. 19, pp. 22098-113, Sep 23 2013, doi: 10.1364/OE.21.022098.

[30] S. D. Johnson, D. B. Phillips, Z. Ma, S. Ramachandran, and M. J. Padgett, "A light-in-flight single-pixel camera for use in the visible and short-wave infrared," *Opt Express,* vol. 27, no. 7, pp. 9829-9837, Apr 1 2019, doi: 10.1364/OE.27.009829.

[31] M. Zohrabi, W. Y. Lim, R. H. Cormack, O. D. Supekar, V. M. Bright, and J. T. Gopinath, "Lidar system with nonmechanical electrowetting-based wide-angle

beam steering," *Opt Express,* vol. 27, no. 4, pp. 4404-4415, Feb 18 2019, doi: 10.1364/OE.27.004404.

[32] K. Ito *et al.*, "System Design and Performance Characterization of a MEMS-Based Laser Scanning Time-of-Flight Sensor Based on a 256 $\times$ 64-pixel Single-Photon Imager," *IEEE Photonics Journal,* vol. 5, no. 2, pp. 6800114-6800114, 2013, doi: 10.1109/jphot.2013.2247586.

[33] M. J. R. Heck, "Highly integrated optical phased arrays: photonic integrated circuits for optical beam shaping and beam steering," *Nanophotonics,* vol. 6, no. 1, pp. 93-107, 2017, doi: 10.1515/nanoph-2015-0152.

[34] J. Zhou and K. Qian, "Low-voltage wide-field-of-view lidar scanning system based on a MEMS mirror," *Appl Opt,* vol. 58, no. 5, pp. A283-A290, Feb 10 2019, doi: 10.1364/AO.58.00A283.

[35] P. K. Choudhury and C.-H. Lee, "Simultaneous Enhancement of Scanning Area and Imaging Speed for a MEMS Mirror Based High Resolution LiDAR," *IEEE Access,* vol. 8, pp. 52113-52120, 2020, doi: 10.1109/access.2020.2979326.

[36] X. Lee and C. Wang, "Optical design for uniform scanning in MEMS-based 3D imaging lidar," *Appl Opt,* vol. 54, no. 9, pp. 2219-23, Mar 20 2015, doi: 10.1364/AO.54.002219.

[37] X. Zhang, S. J. Koppal, R. Zhang, L. Zhou, E. Butler, and H. Xie, "Wide-angle structured light with a scanning MEMS mirror in liquid," *Opt Express,* vol. 24, no. 4, pp. 3479-87, Feb 22 2016, doi: 10.1364/OE.24.003479.

[38] CBC Geospatial Consulting, Inc., "Terrestrial LiDAR 3D Laser Scanning", 2018, http://www.cbcgeospatial.com/terrestrial-lidar.html"

[39] Kathleen Hagen, "U.S. Airborne LiDAR Market Top Impacting Factors", 2016, https://medium.com/@kathleenhagen2/u-s-airborne-lidar-market-top-impacting-

factors-b19def6781c4

[40]   "Advanced   Driver   Assistance   Systems   (ADAS)",   2019,
https://www.youtube.com/watch?v=514-AnwOeGc&app=desktop

[41]   Alan Ohnsman, "Lidar Pioneer Velodyne Debuts $100 Auto Safety Sensor As
Self-Driving   Cars'   Pace   To   Market   Slows",   2020,
https://www.forbes.com/sites/alanohnsman/2020/01/07/lidar-pioneer-velodyne-
debuts-100-auto-safety-sensor-as-self-driving-cars-pace-to-market-
slows/?sh=47b819ae6cbc

[42]   Junko Yoshida, "Lidar Tech Today, Lidar Vendors Tomorrow", 2018,
https://www.eetimes.com/lidar-tech-today-lidar-vendors-tomorrow/

[43]   Bharat Lohani, "Surveillance system based on Flash LiDAR", 2013,
https://www.researchgate.net/publication/261333968_Surveillance_system_base
d_on_Flash_LiDAR

[44]   Quanergy Systems, Inc., https://quanergy.com/products/s3/

[45]   Velodyne, Inc., https://velodynelidar.com/products/

[46]   Infineon, Inc., https://www.infineon.com/

[47]   A. Bauer, E. M. Schiesser, and J. P. Rolland, "Starting geometry creation and
design method for freeform optics," Nat Commun, vol. 9, no. 1, p. 1756, May 1
2018, doi: 10.1038/s41467-018-04186-9.

[48]   T. Yang, G. F. Jin, and J. Zhu, "Automated design of freeform imaging systems,"
Light Sci Appl, vol. 6, no. 10, p. e17081, Oct 2017, doi: 10.1038/lsa.2017.81.

[49]   A. Bauer and J. P. Rolland, "Design of a freeform electronic viewfinder coupled
to aberration fields of freeform optics," Opt Express, vol. 23, no. 22, pp. 28141-
53, Nov 2 2015, doi: 10.1364/OE.23.028141.

[50]   K. Fuerschbach, J. P. Rolland, and K. P. Thompson, "Theory of aberration fields

for general optical systems with freeform surfaces," Opt Express, vol. 22, no. 22, pp. 26585-606, Nov 3 2014, doi: 10.1364/OE.22.026585.

[51] Y. Zhong and H. Gross, "Initial system design method for non-rotationally symmetric systems based on Gaussian brackets and Nodal aberration theory," Opt Express, vol. 25, no. 9, pp. 10016-10030, May 1 2017, doi: 10.1364/OE.25.010016.

[52] T. Gong, G. Jin, and J. Zhu, "Point-by-point design method for mixed-surface-type off-axis reflective imaging systems with spherical, aspheric, and freeform surfaces," Opt Express, vol. 25, no. 9, pp. 10663-10676, May 1 2017, doi: 10.1364/OE.25.010663.

[53] R. Tang, B. Zhang, G. Jin, and J. Zhu, "Multiple surface expansion method for design of freeform imaging systems," Opt Express, vol. 26, no. 3, pp. 2983-2994, Feb 5 2018, doi: 10.1364/OE.26.002983.

[54] T. Yang, J. Zhu, and G. Jin, "Starting configuration design method of freeform imaging and afocal systems with a real exit pupil," Appl Opt, vol. 55, no. 2, pp. 345-53, Jan 10 2016, doi: 10.1364/AO.55.000345.

[55] X. Wu, J. Zhu, T. Yang, and G. Jin, "Transverse image translation using an optical freeform single lens," Appl Opt, vol. 54, no. 28, pp. E55-62, Oct 1 2015, doi: 10.1364/AO.54.000E55.

[56] C. Chen, "Methods of solving aspheric singlets and cemented doublets with given primary aberrations," Appl Opt, vol. 53, no. 29, pp. H202-12, Oct 10 2014, doi:

[57] Robert Fischer, "Optical System Design, Second Edition", McGraw-Hill Education, ISBN-13 : 978-0071472487, 2008

[58] Eugene Hecht, "Optics", Pearson, ISBN-13 : 978-0133977226, 2015

[59] Zemax, Inc., https://www.zemax.com/

[60] Veljko Milanovi, "DEVICE FOR OPTICAL IMAGING, TRACKING, AND POSITION MEASUREMENT WITH ASCANNING MEMS MIRROR", United States Patent, US 8.427,657 B2, 2013

[61] Yew Kwang Low, "WIDE FIELD - OF - VIEW LIDAR OPTICAL ASSEMBLY AND SYSTEM", United States Patent, US 2020/0096643 A1, 2020

[62] Yew Kwang Low," MEMS mirror with extended field of view useful for vehicle lidar", United States Patent, US 2020/0150244 A1, 2020

[63] J. Zhou and K. Qian, "Low-voltage wide-field-of-view lidar scanning system based on a MEMS mirror," Appl Opt, vol. 58, no. 5, pp. A283-A290, Feb 10 2019, doi: 10.1364/AO.58.00A283.

[64] C. Zhu, M. J. Hobbs, M. P. Grainger, and J. R. Willmott, "Design and realization of a wide field of view infrared scanning system with an integrated micro-electromechanical system mirror," Appl Opt, vol. 57, no. 36, pp. 10449-10457, Dec 20 2018, doi: 10.1364/AO.57.010449.

[65] X. Lee, C. Wang, Z. Luo, and S. Li, "Optical design of a new folding scanning system in MEMS-based lidar," Optics & Laser Technology, vol. 125, 2020, doi: 10.1016/j.optlastec.2019.106013.